

TXL Fusion: A Hybrid Machine Learning Framework Integrating Chemical Heuristics and Large Language Models for Topological Materials Discovery

Arif Ullah,^{*,†} Rajibul Islam,[‡] Ghulam Hussain,[¶] Zahir Muhammad,[§] Xiaoguang Li,[¶] and Ming Yang[†]

[†]*School of Physics, Anhui University, Hefei, 230601, Anhui, China*

[‡]*Department of Physics, University of Alabama at Birmingham, Birmingham 35294, AL, USA*

[¶]*Institute for Advanced Study, Shenzhen University, Shenzhen 518060, China*

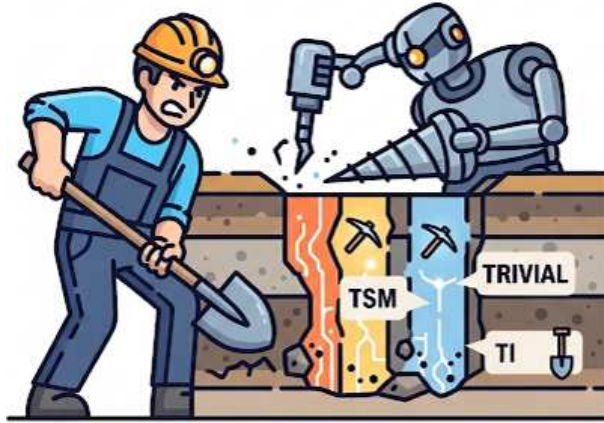
[§]*National Key Laboratory of Spintronics, Hangzhou International Innovation Institute, Beihang University, Hangzhou 311115, China*

E-mail: arif@ahu.edu.cn

Abstract

Topological materials—including insulators (TIs) and semimetals (TSMs)—hold immense promise for quantum technologies, yet their discovery remains constrained by the high computational cost of first-principles calculations and the slow, resource-intensive nature of experimental synthesis. Here, we introduce TXL Fusion, a hybrid machine learning framework that integrates chemical heuristics, engineered physical descriptors, and large language model (LLM) embeddings to accelerate the discovery of topological materials. By incorporating features such as space group symmetry, valence electron

configurations, and composition-derived metrics, TXL Fusion classifies materials across trivial, TSM, and TI categories with improved accuracy and generalization compared to conventional approaches. The framework successfully identified new candidates, with representative cases further validated through density functional theory (DFT), confirming its predictive robustness. By uniting data-driven learning with chemical intuition, TXL Fusion enables rapid and interpretable exploration of complex materials spaces, establishing a scalable paradigm for the intelligent discovery of next-generation topological and quantum materials.



Topological materials, encompassing topological insulators (TIs)^{1,2} and topological semimetals (TSMs),^{3,4} represent unconventional quantum phases of matter characterized by nontrivial electronic band topology. Their robust boundary states, protected against perturbations such as disorder or symmetry breaking, give rise to exotic phenomena including the quantum spin Hall effect,⁵ unusual transport properties,² and magnetoelectric responses.⁶ These unique properties position topological materials as promising candidates for next-generation quantum and spintronic technologies. Since the emergence of the field, a central challenge has been the reliable identification and classification of such materials. Early efforts relied heavily on first-principles calculations combined with topological band theory,^{7,8} a computationally intensive but powerful route for establishing topological order. The advent of symmetry

indicators⁹⁻¹¹ and topological quantum chemistry¹² represented a major milestone, enabling efficient diagnosis of many topological phases directly from symmetry representations of electronic states. These symmetry-based approaches facilitated high-throughput computational searches, resulting in extensive databases of candidate topological materials and accelerating both theoretical and experimental exploration.¹³⁻¹⁵

Despite these advances, symmetry-based methods face inherent limitations. Certain topological phases, such as Chern insulators and time-reversal-invariant Z_2 insulators without point group symmetries, remain invisible to symmetry indicators and require explicit evaluation of wavefunction-based topological invariants, which is computationally expensive.¹¹ Materials with low-symmetry or complex magnetic structures pose additional challenges for symmetry-based diagnosis.¹⁶ As a result, the discovery of topological materials is constrained by computational bottlenecks and the limited scope of existing frameworks.

Over the past decade, machine learning (ML) has become a scalable alternative to symmetry-based approaches for classification and properties prediction of topological materials.¹⁷⁻²⁴ Models such as gradient-boosted trees trained on space group (SG), electron count, and orbital-resolved valence descriptors have achieved strong performance,²⁵ and neural networks applied to computed XANES spectra have further expanded predictive capabilities.²⁶ Despite these advances, conventional ML models operate solely on structured numerical inputs, limiting their ability to incorporate unstructured information—such as material descriptions, experimental annotations, or insights from scientific literature. To overcome data and scalability constraints, composition-based heuristics have been proposed, most notably the topogivity score $g(M)$,²⁷ with subsequent extensions such as the integration of Hubbard U parameter for magnetic systems²⁸ and the inclusion of quantum correlations across elements.²⁹ While efficient and interpretable, these composition-only rules remain insensitive to essential physical features and often struggle to distinguish closely related phases, particularly TSMs and TIs.

Recently, large language models (LLMs) have opened new opportunities by encoding

chemical knowledge from vast scientific corpora. Unlike conventional descriptor-based ML, LLMs capture contextual relationships and support few-shot learning without manual feature engineering. Their versatility spans fine-tuning for chemistry Q & A,³⁰ hybrid embedding with graph neural networks,³¹ synthesis prediction,³² chatbot-assisted quantum chemistry,³³ dataset curation,³⁴ AI-driven simulation assistants,³⁵ and crystalline property prediction with transformer architectures.^{36,37} Beyond prediction, LLM embeddings provide compositional and structural representations that enable similarity search, candidate retrieval, and multi-task learning,³⁸ while fine-tuning on text-encoded atomistic data has shown promise in generating physically stable structures.³⁹

Despite recent advances, the use of LLMs in the discovery and categorization of topological materials remains largely underexplored. To bridge this gap, we introduce TXL Fusion, a hybrid framework that unites three complementary pillars: (i) composition-driven chemical heuristics, (ii) domain-specific numerical descriptors, and (iii) embeddings derived from a fine-tuned LLM. By leveraging the strengths of these distinct sources, TXL Fusion delivers higher accuracy, robustness, and generalization than any single method alone. The framework enables high-throughput screening of unexplored chemical spaces, identifying numerous potential topological materials, with a subset of low-cost cases further validated through density functional theory (DFT) calculations. Our results demonstrate that combining symbolic, statistical, and linguistic knowledge provides a powerful paradigm for addressing complex discovery challenges in materials science.

Dataset and Feature Selection

We source our data from the topological materials database,^{12,13,40–42} which includes DFT calculations with spin-orbit coupling (SOC) on 38,184 materials, comprising 6,109 TIs ($\sim 16\%$), 13,985 TSMs ($\sim 36.6\%$), and 18,090 trivial materials ($\sim 47.3\%$). Guided by both theoretical considerations and systematic empirical analysis, we conduct a comprehensive feature selec-

tion process where our initial feature set spanned over many properties including chemical bonding characteristics (e.g., covalent vs. ionic tendencies), SOC strength ($\propto Z^4$), periodic table’s group and column positions, total number of electrons, SG, valence electrons and atomic mass. Through iterative evaluation, we refine this broad feature pool to a compact set of descriptors that consistently offered both statistical robustness and physical interpretability. Further methodological details and extended analysis are provided in Section S1 of Supporting Information. Based on our analyses, SG symmetry emerged as the most decisive indicator of topological character. High-symmetry cubic and tetragonal SGs (e.g., 194, 225, 221, 139) are predominantly associated with TSMs, while low-symmetry monoclinic and orthorhombic SGs (e.g., 14, 62, 15) favor trivial compounds. TIs occupy intermediate symmetry regimes (e.g., 62, 63, 139), indicating that symmetry constraints are necessary but not sufficient for topological behavior. Several SGs are entirely absent in specific classes, confirming strong symmetry selectivity across topological phases (Supporting Information, Fig. S1 and Table S1).

Complementary chemical and electronic descriptors further enhance class separability. TIs show enriched d- and f-orbital participation and higher transition-metal and lanthanide content, consistent with strong SOC and band inversion. Trivial compounds, by contrast, are dominated by nonmetals and p-orbital bonding, reflecting localized, covalent environments. Electron-count parity further differentiates metallic from insulating systems: 70.7% of TSMs possess odd electron counts, enforcing metallicity via Kramers degeneracy, while most TIs and trivials exhibit even counts that permit full band filling. Bonding analysis reveals that TIs and TSMs preferentially adopt mostly covalent character, whereas trivials are more ionic, underscoring the role of delocalized orbitals in stabilizing nontrivial topology (Supporting Information, Table S2).

Collectively, these insights establish a concise and interpretable feature space—integrating symmetry, orbital, compositional, and bonding descriptors—that forms the foundation of our TXL Fusion framework presented below.

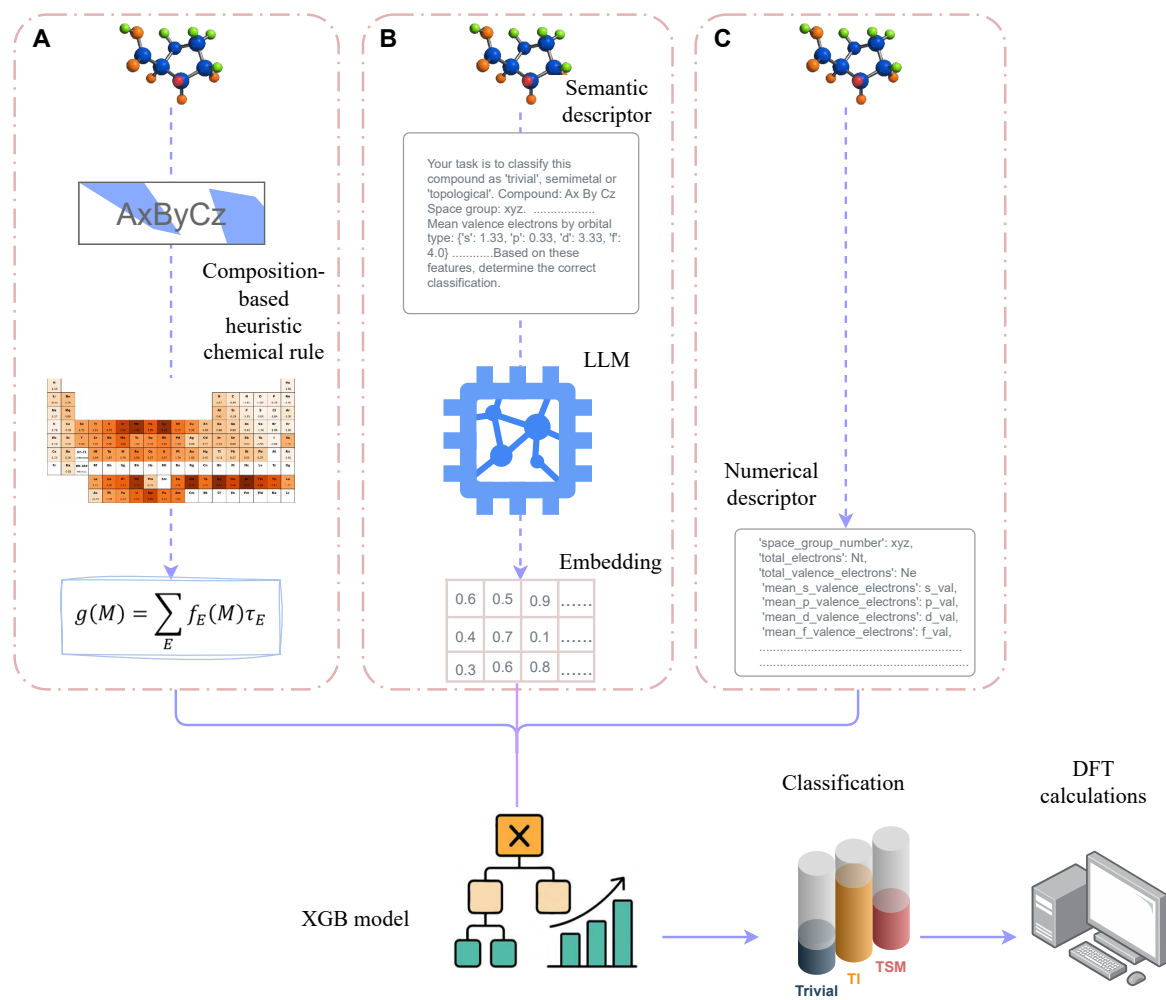


Figure 1: Schematic flowchart of the TXL Fusion model, outlining the main stages of the workflow.

TXL Fusion architecture

The TXL Fusion model integrates chemically inspired heuristics, numerical descriptors, and LLM embeddings within a unified hybrid framework that couples domain intuition with data-driven learning for robust classification of topological materials. As illustrated in Fig. 1, the framework consists of three interconnected modules, each detailed in the Supporting Information (Section S2).

The pipeline begins with a composition-based heuristic module, adapted from Ma et al.,²⁷ which assigns elemental contribution scores to estimate the likelihood of a material being trivial, TSM, or a TI. This heuristic captures global compositional trends consistent with chemical intuition—where lighter, nonmetallic elements favor trivial phases, while heavier elements such as Bi, Sb, and Te correlate with topological behavior. However, since heuristic trends alone cannot distinguish between TIs and TSMs (see Table 1 in the "Results and Discussion" section), we complement it by numerical descriptor module.

The numerical descriptor module encodes physically meaningful quantities—such as SG symmetry, total and parity-resolved electron counts, orbital occupancies, electronegativity differences, and compositional ratios—into a fixed-length vector. These descriptors, selected through the feature analysis described in Section "Dataset and Feature Selection" and Supporting Information (Section S1), provide a systematic and interpretable representation of the material’s underlying physics.

The third component in our pipeline is LLM embedding module, built upon a fine-tuned SciBERT encoder, converts structured textual descriptions of materials (including chemical formulas, SG annotations, orbital contributions, and heuristic-derived reasoning) into dense semantic embeddings. These embeddings capture contextual and higher-order correlations beyond what explicit numerical features represent, linking symbolic chemical knowledge with statistical learning.

Finally, the heuristic outputs, numerical descriptors, and LLM embeddings are concatenated to form a comprehensive feature representation, which is passed to an eXtreme Gra-

dient Boosting (XGB) classifier for final prediction. This multi-layered integration enables TXL Fusion to balance interpretability and performance, offering a scalable, generalizable approach for the intelligent discovery of topological materials. Detailed implementation procedures and model specifications are provided in the Supporting Information (Sections S2-3).

Results and Discussion

In this section, we assess the capability of the proposed TXL Fusion model to distinguish topological materials from trivial ones and benchmark it against two standalone baselines: the composition-based heuristic rule $g(M)$ and a numerical descriptor-based XGB model. Detailed training procedures are provided in the Supporting Information (Section S3). The dataset was divided into 80% for training and 20% for testing (7637 materials), with the latter designated as Discovery Space-1, on which high-throughput screening was conducted using features learned from the training data. The training subset was further partitioned into 80% sub-training and 20% validation data; no validation results are reported for $g(M)$ since it represents a fixed analytical rule. Model performance is evaluated using precision, recall, and F1-score:

$$\text{Precision} = \frac{TP}{TP + FP}, \quad \text{Recall} = \frac{TP}{TP + FN}, \quad \text{F1} = 2 \cdot \frac{\text{Precision} \cdot \text{Recall}}{\text{Precision} + \text{Recall}}, \quad (1)$$

where TP , FP , and FN denote true positives, false positives, and false negatives. Precision reflects the fraction of predicted positives that are correct, recall measures the fraction of true positives recovered, and F1-score balances the two.

Table 1 summarizes comparative performance on 7637 unseen materials of Discovery Space-1. The $g(M)$ rule, while interpretable and chemically motivated, performs poorly in Discovery Space-1: although $g(M)^{\text{Trivial-Others}}$ distinguishes trivial compounds reasonably well (F1 = 0.81), it performs worse on TSMs (F1 = 0.62) and fails entirely for TIs (F1 =

0.00), reflecting its reliance on composition vectors alone. The numerical descriptor based XGB model, leveraging richer numerical and structural features, outperforms $g(M)$ rule for TI and TSM classification ($F1 > 0.85$ across splits) but still struggles with TIs ($F1 = 0.57$ in Discovery Space-1), limited by its factorized nature, which treats features such as SG, electron count, orbital occupations, and elemental ratios as independent scalars.

By contrast, TXL Fusion consistently outperforms the baselines across all classes, achieving F1 scores of 0.89 (trivial), 0.89 (TSM), and 0.62 (TI). This represents a clear improvement over XGB, particularly for TIs by +5%. This superior performance stems from its hybrid design, with its primary advantage arising from LLM embeddings that capture complex, coupled electronic–structural correlations, allowing the model to surpass the limitations of factorized numerical descriptors. A detailed comparison of semantic versus numerical descriptors, highlighting these advantages, is provided in Section S4 of the Supporting Information.

It is worth mentioning that performance varies with chemical complexity (Supporting Information Section S5). For single-element compounds, both TXL and XGB struggle with TIs ($F1 < 0.25$) due to data scarcity, limited descriptor variability, and subtle, non-compositional physical effects. Accuracy improves for 2–3 element compounds, where TXL slightly outperforms XGB ($F1 \approx 0.62$ – 0.64 vs. 0.59 – 0.63). The largest advantage appears for 4–5 element systems, where TXL sustains reliable TI predictions ($F1 = 0.57$ – 0.61) while XGB sharply underperforms ($F1 = 0.24$ – 0.31). For six-element compounds—the most sparsely represented category in the dataset—TXL Fusion retains better balance for rare TI cases ($F1 = 0.33$ compared to 0.00 for XGB), while both models achieve strong performance for trivial and TSM classes.

Calibration results (Supporting Information Section S5) show that TXL Fusion is most reliable at higher confidence levels: predictions above 90% confidence are nearly always correct across all classes, supported by sufficient sample counts. In contrast, predictions in the 30–50% range are less dependable, with accuracies often below bin midpoints, indicat-

ing overconfidence. This is most evident in the 30–40% range, where trivial predictions show perfect accuracy but are based on only three samples, rendering the result statistically insignificant.

Finally, feature importance analysis (Fig. 2) highlights TXL Fusion’s advantage. While the numerical descriptor-based XGB model depends heavily on electron parity, SG probabilities, and p-valence counts, TXL Fusion derives balanced contributions from $g(M)$ scores and LLM embeddings. This integration of interpretability, engineered robustness, and contextual depth underlies TXL Fusion’s superior generalization in discovery-oriented test spaces.

Table 1: Comparison of classification performance for the chemical rule $g(M)$, the numerical descriptor based XGB, and TXL Fusion models on the validation set and Discovery Space-1. The chemical rules $g(M)^{\text{Trivial-Others}}$, $g(M)^{\text{TSM-Others}}$ and $g(M)^{\text{TI-Others}}$ represent two-label classification tasks distinguishing trivial, TSM, and TI compounds from the other classes, respectively. Metrics are reported as precision, recall, and F1-score for each class.

Model	Class	Validation Set			Discovery Space-1		
		Precision	Recall	F1	Precision	Recall	F1
$g(M)^{\text{Trivial-Others}}$	Trivial				0.87	0.77	0.81
	Others				0.77	0.87	0.81
$g(M)^{\text{TSM-Others}}$	TSM				0.65	0.60	0.62
	Others				0.78	0.81	0.80
$g(M)^{\text{TI-Others}}$	TI				0.00	0.00	0.00
	Others				0.83	1.00	0.90
XGB model	Trivial	0.88	0.91	0.89	0.87	0.90	0.88
	TSM	0.84	0.89	0.86	0.82	0.88	0.85
	TI	0.66	0.49	0.56	0.67	0.50	0.57
TXL Fusion	Trivial	0.90	0.91	0.91	0.88	0.91	0.89
	TSM	0.88	0.87	0.89	0.85	0.87	0.86
	TI	0.68	0.63	0.65	0.67	0.58	0.62

To further evaluate the TXL Fusion’s predictive capability, we used the set of 1,433 materials reported in Ma et al.²⁷ as a discovery space. These materials, originally curated by Tang et al.,¹⁵ are of particular interest because their topological character cannot be resolved using symmetry indicators. Among them, 1,235 compounds are already present in the topological materials database, leaving 198 as a new testing set, which we refer to as

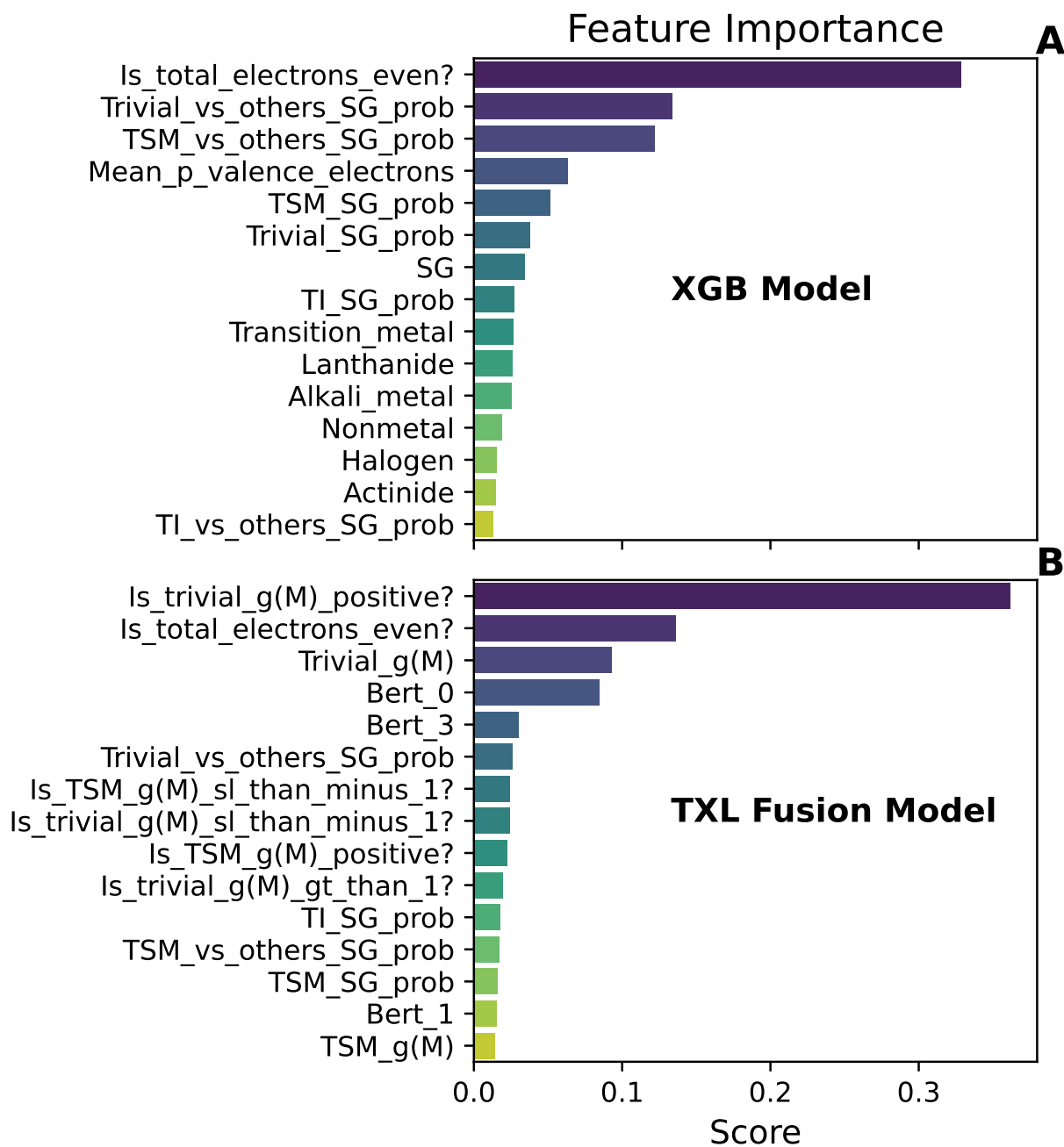


Figure 2: Feature importance in material classification for (A) the numerical descriptor-based XGB model and (B) the TXL Fusion model. Here Bert_n ($n = 1, \dots, 5$) denotes the five principal components derived from principal component analysis (PCA) of the 768-dimensional embeddings obtained from the fine-tuned LLM.

Discovery Space-2. Two compounds belonging to SG 178 were excluded, as this SG is not represented in the topological materials database, resulting in 196 candidate materials.

From these 196 candidates, our TXL Fusion model identified 21 potential TSMs with varying confidence levels: $\text{Li}_{22}\text{Pb}_5$ (216), $\text{Bi}_2\text{Cl}_7\text{Se}_5$ (19), $\text{Cl}_{11}\text{Mo}_3\text{N}_2$ (29), $\text{Li}_{22}\text{Sn}_5$ (216), AgPb_4Pd_6 (152), NS_2 (102), SbO_2 (33), $\text{P}_3\text{Rb}_2\text{Se}_6$ (29), RbSO_3 (150), LaMo_2O_5 (186), TlC_2O_2 (19), $\text{Ta}_{21}\text{Te}_{13}$ (183), OTi_6 (159), CNSe (19), RbGe_8Li_7 (186), $\text{Ag}_{10}\text{Br}_3\text{Te}_4$ (36), $\text{Cs}_9\text{O}_3\text{Tl}_4$ (197), C_8Cs (191), $\text{In}_{11}\text{Mo}_{40}\text{O}_{62}$ (26), BiSe_3Sr (19), $\text{Ge}_5\text{Li}_{22}$ (216), P_3Sc_7 (186).

Among these, $\text{In}_{11}\text{Mo}_{40}\text{O}_{62}$ (26) and AgPb_4Pd_6 (152) were flagged as TSMs but could not be located in the materials project database⁴³ and were thus excluded. For the remaining 19 predicted TSMs, DFT calculations were carried out on five representative compounds (CsC_8 (191), OTi_6 (159), SbO_2 (33), NS_2 (102), and P_3Sc_7 (186)), while the others were omitted due to the high computational cost (see Supporting Information Section S6 for computational details).

As shown in Fig. 3, among the five tested compounds—four (CsC_8 , OTi_6 , SbO_2 , and P_3Sc_7) were validated as TSMs, suggesting an estimated success rate of approximately 80% if extrapolated to the full set. Specifically, as shown in Fig. 3, CsC_8 (191) exhibits graphite-derived dispersions with weak SOC, maintaining a trivial character, while OTi_6 (159) displays broad metallic states without inversion. SbO_2 (33), despite containing the heavy pnictogen Sb, shows complex near-metallic behavior with small gaps and pseudogaps across the Brillouin zone. P_3Sc_7 (186) features dispersive metallic bands consistent with trivial metallicity. These results demonstrate that the TXL Fusion model accurately captures the topological nature of materials directly from elemental and compositional features, highlighting its strong predictive capability and potential as a scalable framework for data-driven topological materials discovery.

Concluding remarks

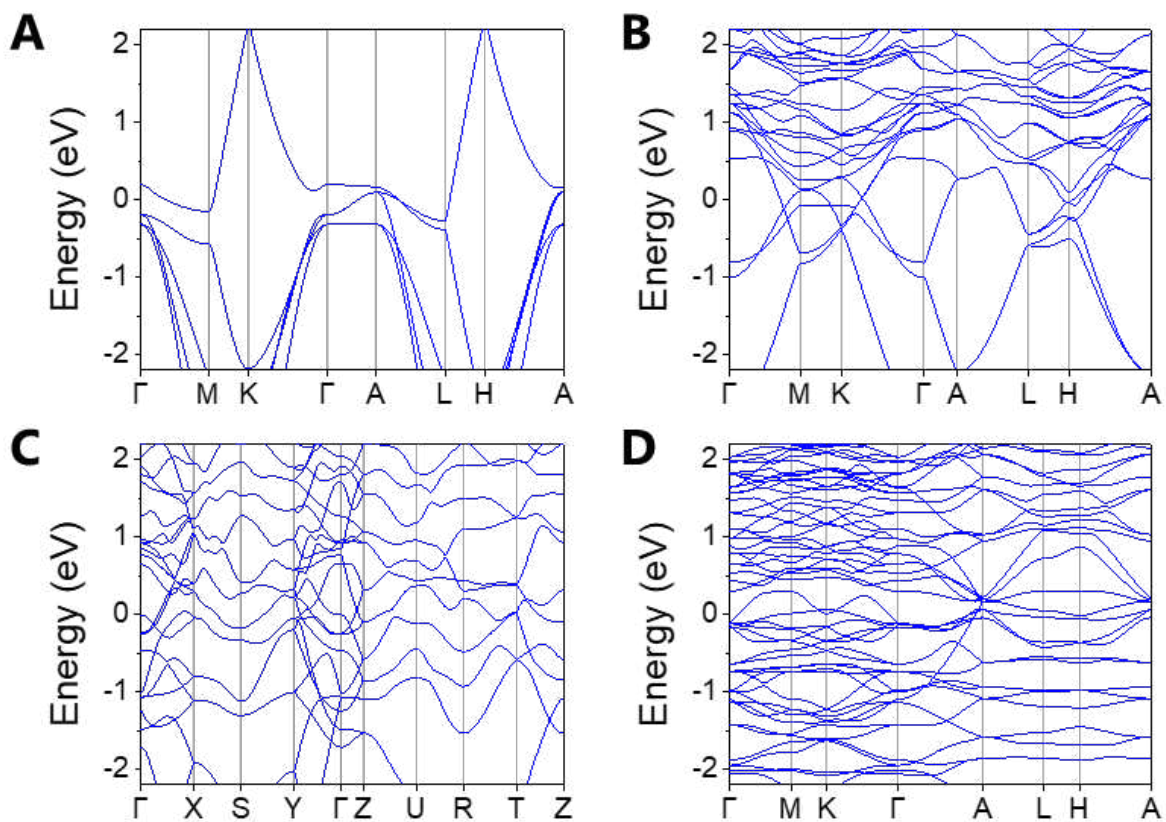


Figure 3: Electronic band structures along with space groups (A) CsC_8 (191), (B) OTi_6 (159), (C) SbO_2 (33) and (D) P_3Sc_7 (186).

In this work, we introduced TXL Fusion, a hybrid framework that integrates chemically informed heuristics, numerical descriptors, and LLM-derived semantic embeddings for robust classification of topological materials. Across all classes, TXL Fusion consistently surpasses both the standalone XGB model and the heuristic $g(M)$ rule, demonstrating the effectiveness of combining domain intuition with data-driven, context-aware representations. By unifying interpretable chemical trends with high-dimensional semantic embeddings, the model achieves improved accuracy and generalization, particularly for compositionally complex systems. To promote broader community access, TXL Fusion will be made publicly available through the Aitomistic Hub at aitomistic.xyz.

Despite these advances, several intrinsic challenges remain. TIs are the most difficult class to predict, primarily due to label uncertainty and data sparsity. As discussed in Section S7 of the Supporting Information, DFT-based topological labels—especially for small-gap or borderline systems—can be unreliable, effectively introducing noise into the training data. Consistent with this interpretation, evaluation on high-confidence TI subsets shows systematic performance improvements as label reliability increases (Fig. S7). In addition, element-resolved analysis in Section S5 reveals reduced performance for low-complexity compounds (single- and binary-element systems), arising from a combination of data scarcity, limited descriptor expressiveness due to compositional features collapsing to constants or narrow ranges, and the dominance of subtle, non-compositional physical effects (see Section S5.1).

While these limitations could be mitigated by incorporating more localized or symmetry-resolved physical descriptors—such as symmetry-indicator eigenvalues, band inversion indicators, Wannier charge centers, or orbital-projected band-edge features—such quantities are computationally intensive and not uniformly available at scale. Within our framework, we therefore prioritize broad chemical coverage, enabling large-scale screening based solely on elemental information without requiring prior expensive calculations.

At the same time, TXL Fusion demonstrates strong generalization under chemical spar-

sity. As detailed in Section S5.2, the model maintains reliable performance for trivial and TSM phases even in sparsely sampled or partially out-of-distribution chemical families, with its advantage over numerical baselines increasing alongside chemical and electronic complexity. Moreover, confidence-based calibration analysis (Section S5) shows that TXL Fusion is well calibrated at high confidence levels, indicating that its most confident predictions are highly reliable and well suited for guiding experimental validation.

More broadly, this study highlights the power of LLM-based semantic embeddings for materials discovery. As discussed in Section S4, these embeddings capture coupled electronic–structural relationships that are fragmented in conventional factorized numerical descriptors, enabling improved discrimination of subtle topological regimes. Looking forward, continued improvements in label fidelity, expanded high-confidence datasets, and the incorporation of additional physics-aware learning strategies—such as transfer learning across chemical families or cost-sensitive training to address class imbalance—are expected to further enhance performance. More generally, the TXL Fusion framework is not limited to topological materials and provides a flexible foundation for accelerating discovery across a broad range of quantum and functional materials systems.

Acknowledgement

A.U. acknowledges funding from the National Natural Science Foundation of China (No. W2433037) and the Natural Science Foundation of Anhui Province (No. 2408085QA002).

Code and Data Availability

Code and data are available at https://github.com/Arif-PhyChem/txl_fusion

Supporting Information Available

Comprehensive methodology and supplementary analyses—including feature engineering, TXL Fusion architecture and training details, a semantic versus numerical descriptor performance comparison, element-resolved performance and confidence analysis with dedicated discussions of low-complexity compounds and chemical sparsity generalization, DFT computational settings, and an assessment of noise and reliability in DFT-based topological labels—are provided in the Supporting Information (Sections S1–S7).

References

- (1) Hasan, M. Z.; Kane, C. L. Colloquium: Topological insulators. *Rev. Mod. Phys.* **2010**, *82*, 3045–3067.
- (2) Qi, X.-L.; Zhang, S.-C. Topological insulators and superconductors. *Rev. Mod. Phys.* **2011**, *83*, 1057–1110.
- (3) Liu, Z. K.; Zhou, B.; Zhang, Y.; Wang, Z. J.; Weng, H. M.; Prabhakaran, D.; Mo, S.-K.; Shen, Z. X.; Fang, Z.; Dai, X.; Hussain, Z.; Chen, Y. L. Discovery of a Three-Dimensional Topological Dirac Semimetal, Na_3Bi . *Science* **2014**, *343*, 864–867.
- (4) Xu, S.-Y. et al. Discovery of a Weyl fermion semimetal and topological Fermi arcs. *Science* **2015**, *349*, 613–617.
- (5) Kane, C. L.; Mele, E. J. Quantum Spin Hall Effect in Graphene. *Phys. Rev. Lett.* **2005**, *95*, 226801.
- (6) Hu, J.; Xu, S.-Y.; Ni, N.; Mao, Z. Transport of Topological Semimetals. *Annual Review of Materials Research* **2019**, *49*, 207–252.
- (7) Xiao, J.; Yan, B. First-principles calculations for topological quantum materials. *Nature Reviews Physics* **2021**, *3*, 283–297.

- (8) Bansil, A.; Lin, H.; Das, T. Colloquium: Topological band theory. *Rev. Mod. Phys.* **2016**, *88*, 021004.
- (9) Slager, R.-J.; Mesaros, A.; Juričić, V.; Zaanen, J. The space group classification of topological band-insulators. *Nature Physics* **2013**, *9*, 98–102.
- (10) Kruthoff, J.; De Boer, J.; Van Wezel, J.; Kane, C. L.; Slager, R.-J. Topological classification of crystalline insulators through band structure combinatorics. *Physical Review X* **2017**, *7*, 041069.
- (11) Po, H. C.; Vishwanath, A.; Watanabe, H. Symmetry-based indicators of band topology in the 230 space groups. *Nature Communications* **2017**, *8*, 50.
- (12) Bradlyn, B.; Elcoro, L.; Cano, J.; Vergniory, M. G.; Wang, Z.; Felser, C.; Aroyo, M. I.; Bernevig, B. A. Topological quantum chemistry. *Nature* **2017**, *547*, 298–305.
- (13) Vergniory, M.; Elcoro, L.; Felser, C.; Regnault, N.; Bernevig, B. A.; Wang, Z. A complete catalogue of high-quality topological materials. *Nature* **2019**, *566*, 480–485.
- (14) Zhang, T.; Jiang, Y.; Song, Z.; Huang, H.; He, Y.; Fang, Z.; Weng, H.; Fang, C. Catalogue of topological electronic materials. *Nature* **2019**, *566*, 475–479.
- (15) Tang, F.; Po, H. C.; Vishwanath, A.; Wan, X. Comprehensive search for topological materials using symmetry indicators. *Nature* **2019**, *566*, 486–489.
- (16) Xu, Y.; Elcoro, L.; Song, Z.-D.; Wieder, B. J.; Vergniory, M. G.; Regnault, N.; Chen, Y.; Felser, C.; Bernevig, B. A. High-throughput calculations of magnetic topological materials. *Nature* **2020**, *586*, 702–707.
- (17) Zhang, P.; Shen, H.; Zhai, H. Machine Learning Topological Invariants with Neural Networks. *Phys. Rev. Lett.* **2018**, *120*, 066401.
- (18) Scheurer, M. S.; Slager, R.-J. Unsupervised Machine Learning and Band Topology. *Phys. Rev. Lett.* **2020**, *124*, 226401.

- (19) Cao, G.; Ouyang, R.; Ghiringhelli, L. M.; Scheffler, M.; Liu, H.; Carbogno, C.; Zhang, Z. Artificial intelligence for high-throughput discovery of topological insulators: The example of alloyed tetradymites. *Physical Review Materials* **2020**, *4*, 034204.
- (20) Choudhary, K.; Garrity, K. F.; Ghimire, N. J.; Anand, N.; Tavazza, F. High-throughput search for magnetic topological materials using spin-orbit spillage, machine learning, and experiments. *Phys. Rev. B* **2021**, *103*, 155131.
- (21) Schleder, G. R.; Focassio, B.; Fazzio, A. Machine learning for materials discovery: Two-dimensional topological insulators. *Applied Physics Reviews* **2021**, *8*, 031409.
- (22) Tyner, A. C. Machine learning guided discovery of stable, spin-resolved topological insulators. *Physical Review Research* **2024**, *6*, 023316.
- (23) Hong, T.; Chen, T.; Jin, D.; Zhu, Y.; Gao, H.; Zhao, K.; Zhang, T.; Ren, W.; Cao, G. Discovery of new topological insulators and semimetals using deep generative models. *npj Quantum Materials* **2025**, *10*, 12.
- (24) Haosheng, X.; Dongheng, Q.; Jing, W. Predicting Many Crystal Properties via an Adaptive Transformer-based Framework. *Chin. Phys. Lett.* **2025**, *42*, 070706.
- (25) Claussen, N.; Bernevig, B. A.; Regnault, N. Detection of topological materials with machine learning. *Physical Review B* **2020**, *101*, 245117.
- (26) Andrejevic, N.; Andrejevic, J.; Bernevig, B. A.; Regnault, N.; Han, F.; Fabbris, G.; Nguyen, T.; Drucker, N. C.; Rycroft, C. H.; Li, M. Machine-Learning Spectral Indicators of Topology. *Advanced Materials* **2022**, *34*, 2204113.
- (27) Ma, A.; Zhang, Y.; Christensen, T.; Po, H. C.; Jing, L.; Fu, L.; Soljatic, M. Topogivity: A machine-learned chemical rule for discovering topological materials. *Nano Letters* **2023**, *23*, 772–778.

- (28) Xu, H.; Jiang, Y.; Wang, H.; Wang, J. Discovering two-dimensional magnetic topological insulators by machine learning. *Physical Review B* **2024**, *109*, 035122.
- (29) Xu, X.; Islam, R.; Hussain, G.; Huang, Y.; Li, X.; Dral, P. O.; Ullah, A.; Yang, M. Quantum-inspired Chemical Rule for Discovering Topological Materials. *arXiv preprint arXiv:2512.13115* **2025**,
- (30) Jablonka, K. M.; Schwaller, P.; Ortega-Guerrero, A.; Smit, B. Leveraging large language models for predictive chemistry. *Nature Machine Intelligence* **2024**, *6*, 161–169.
- (31) Li, Y.; Gupta, V.; Kilic, M. N. T.; Choudhary, K.; Wines, D.; Liao, W.-k.; Choudhary, A.; Agrawal, A. Hybrid-LLM-GNN: integrating large language models and graph neural networks for enhanced materials property prediction. *Digital Discovery* **2025**, *4*, 376–383.
- (32) Kim, S.; Jung, Y.; Schrier, J. Large Language Models for Inorganic Synthesis Predictions. *Journal of the American Chemical Society* **2024**, *146*, 19654–19659.
- (33) Gadde, R. S. K.; Devaguptam, S.; Ren, F.; Mittal, R.; Dong, L.; Wang, Y.; Liu, F. Chatbot-assisted quantum chemistry for explicitly solvated molecules. *Chem. Sci.* **2025**, *16*, 3852–3864.
- (34) Kang, Y.; Lee, W.; Bae, T.; Han, S.; Jang, H.; Kim, J. Harnessing Large Language Models to Collect and Analyze Metal–Organic Framework Property Data Set. *Journal of the American Chemical Society* **2025**, *147*, 3943–3958.
- (35) Hu, J.; Nawaz, H.; Rui, Y.; Chi, L.; Ullah, A.; Dral, P. O. Aitomia: Your Intelligent Assistant for AI-Driven Atomistic and Quantum Chemical Simulations. 2025; <https://arxiv.org/abs/2505.08195>.
- (36) Niyongabo Rubungo, A.; Arnold, C.; Rand, B. P.; Dieng, A. B. LLM-Prop: predicting

- the properties of crystalline materials using large language models. *npj Computational Materials* **2025**, *11*, 186.
- (37) Korolev, V.; Protsenko, P. Accurate, interpretable predictions of materials properties within transformer language models. *Patterns* **2023**, *4*, 100803.
- (38) Qu, J.; Xie, Y. R.; Ciesielski, K. M.; Porter, C. E.; Toberer, E. S.; Ertekin, E. Leveraging language representation for materials exploration and discovery. *npj Computational Materials* **2024**, *10*, 58.
- (39) Gruver, N.; Sriram, A.; Madotto, A.; Wilson, A. G.; Zitnick, L. C.; Ulissi, Z. Fine-Tuned Language Models Generate Stable Inorganic Materials as Text. 2024; <https://arxiv.org/abs/2402.04379>, preprint.
- (40) Topological Materials Database. <https://www.topologicalquantumchemistry.org/#/>.
- (41) Bilbao Crystallographic Server. <https://www.cryst.ehu.es/>.
- (42) Vergniory, M. G.; Wieder, B. J.; Elcoro, L.; Parkin, S. S.; Felser, C.; Bernevig, B. A.; Regnault, N. All topological bands of all nonmagnetic stoichiometric materials. *Science* **2022**, *376*, eabg9094.
- (43) Horton, M. K. et al. Accelerated data-driven materials science with the Materials Project. *Nature Materials* **2025**, published online 14 April 2025.

Supporting Information for TXL Fusion: A Hybrid Machine Learning Framework Integrating Chemical Heuristics and Large Language Models for Topological Materials Discovery

ARIF ULLAH^{1,*}, RAJIBUL ISLAM², GHULAM HUSSAIN³, ZAHIR MUHAMMAD⁴,
XIAOGUANG LI³, AND MING YANG¹

¹*School of Physics, Anhui University, Hefei, 230601, Anhui, China*

²*Department of Physics, University of Alabama at Birmingham, Birmingham 35294, AL,
USA*

³*Institute for Advanced Study, Shenzhen University, Shenzhen 518060, China*

⁴*National Key Laboratory of Spintronics, Hangzhou International Innovation Institute,
Beihang University, Hangzhou 311115, China*

**Corresponding author: arif@ahu.edu.com*

Table of Contents

S1 Features Analysis	2
S2 Details of the TXL Fusion framework	4
S2.1 Composition-based heuristic chemical rule module	4
S2.2 Numerical descriptor module	9
S2.3 LLM: Semantic descriptor based module	10
S3 Training details	11
S3.1 Composition-based heuristic chemical rule	11
S3.2 Standalone XGB model	12
S3.3 Finetuning of LLM for TXL Fusion	12
S3.4 Training of TXL Fusion	12
S4 Semantic versus numerical descriptor: performance comparison	13
S5 Element-resolved performance and confidence analysis	16
S5.1 Origins of reduced performance in low-complexity compounds	16
S5.2 Generalization of TXL Fusion under chemical sparsity	21
S6 DFT computational details	22

S1 Features Analysis

As mentioned in the main text, we source our data from the topological materials database,^{1–5} which includes spin–orbit coupling (SOC) calculations on 38,184 materials, comprising 6,109 TIs (~16%), 13,985 TSMs (~36.6%), and 18,090 trivial materials (~47.3%). This large and diverse dataset spans a wide range of chemical and structural classes, offering not only a robust ground for analyzing physically motivated descriptors, but more importantly, a comprehensive benchmark for developing advanced ML pipelines. To ensure that our models are both accurate and interpretable, we began by evaluating which physical features most meaningfully differentiate TIs, TSMs, and trivials.

Guided by both theoretical considerations and systematic empirical analysis, we conducted a comprehensive feature selection process where our initial feature set spanned over many properties including chemical bonding characteristics (e.g., covalent vs. ionic tendencies), spin–orbit coupling strength ($\propto Z^4$), periodic table’s group and column positions, total number of electrons, SG, valence electrons and atomic mass. Through iterative evaluation, we refined this broad feature pool to a compact set of descriptors that consistently offered both statistical robustness and physical interpretability.

Among these, SG symmetry emerged as the most decisive feature, playing a pivotal role in determining the likelihood of a compound exhibiting topological, semimetallic, or trivial electronic behavior. Across all datasets, a total of 216 unique SGs are represented. Analyzing the SG with the maximum predicted class probability reveals distinct patterns of symmetry preference among different material classes. As shown in Fig. S1, for trivial compounds, the most frequently assigned SGs are 14 (11.8%), 62 (8.9%), 2 (7.0%), and 15 (6.4%), indicating a strong bias toward lower-symmetry or monoclinic/orthorhombic structures. In contrast, TSMs show peak probabilities in SGs such as 194 (8.0%), 225 (7.9%), 221 (7.6%), and 139 (6.4%), which are typically associated with high-symmetry cubic or tetragonal structures. TIs, meanwhile, most frequently appear in space groups 62 (11.2%), 139 (8.1%), 63 (7.6%), and 12 (7.1%), indicating a nuanced balance between symmetry richness and topological permissiveness.

Crucially, Table S1 identifies a number of SGs that are entirely absent in one or more material classes, reflecting symmetry settings that are incompatible with certain electronic phases. For instance, SGs 196, 103, 106, 175, 210, and 211 are never associated with trivial compounds. Similarly, 32 SGs—including 3, 16, 17, 22, 24, 145, 151, and 153—are never linked to semimetallic behavior. Most strikingly, 118 SGs do not host a single topological compound (e.g., 1–9, 16–46, 75–81, 90–92, 94–100, 102–110, 150–161, 210–214; see Table S1 for the full list), highlighting the strong symmetry-selectivity of topological phases.

Yet, not all SGs act as exclusive indicators. Fig. S1 further reveals that several SGs—such as 62, 63, 166, and 194—span multiple classes, indicating symmetry environments that are permissive to various electronic behaviors depending on additional microscopic factors. For example, SGs like 225, 227, 129, and 139 are frequently shared between trivials and TSMs but rarely host topological ones, hinting at symmetry settings favoring metallicity or conventional band structures. Conversely,

SGs like 2, 12, and 14 appear in both trivial and topological materials, suggesting that symmetry alone is often necessary but not sufficient to determine topological character.

To complement symmetry, we broadened our analysis to include chemical and electronic descriptors beyond symmetry, as summarized in Table S2. Among these, orbital occupancy patterns emerge as highly informative in distinguishing TIs from trivial and TSM classes. Notably, 31.0% of TIs exhibit simultaneous d- and f-orbital occupancy, compared to 6.9% in trivial compounds and 29.0% in TSMs. This co-occupancy reflects enhanced SOC and complex orbital hybridization, conditions theoretically linked to band inversion and nontrivial topology. These observations are further supported by the average valence electron counts: TIs display substantially enhanced d-electron contributions (2.18) relative to trivial materials (0.81), though slightly lower than those of TSMs (2.48). For f-electrons, TIs exhibit a moderate increase over trivial compounds (0.76 vs. 0.13), while remaining marginally lower than TSMs (0.80), indicating that f-orbital involvement is important but not uniquely dominant in insulating topological phases. In contrast, p-orbital occupancy is reduced in TIs (1.35) and TSMs (1.20) compared to trivial materials (2.47), suggesting a departure from simple covalent bonding toward more correlated, relativistic electronic environments. Meanwhile, s-orbital contributions remain relatively consistent across all classes (~ 1.8), indicating that the distinctions in topological behavior are primarily driven by d-, f-, and p-orbital patterns.

In addition to orbital features, elemental composition provides key insights into the electronic character of materials. Both TIs and TSMs are enriched in transition metals (32.8% and 36.8%, respectively) and lanthanides (9.6% and 10.4%), elements with strong SOC and high-angular-momentum orbitals that facilitate band inversion and nontrivial topology. In contrast, trivial materials contain far fewer of these elements—11.9% transition metals and 2.1% lanthanides—consistent with weaker relativistic effects and simpler electronic structures.

The metalloid content also follows a similar pattern: TIs (15.9%) and TSMs (11.5%) exceed trivial compounds (8.3%), reflecting their role in introducing intermediate bonding character and enhancing electronic complexity. Conversely, nonmetals dominate trivial materials (47.4%) but are substantially less prevalent in TIs (21.3%) and TSMs (18.8%), suggesting that strongly covalent environments correlate with trivial phases, whereas topologically nontrivial systems favor heavier, more metallic elements with delocalized electrons and significant SOC.

Other elemental groups—including alkali metals, alkaline earth metals, and actinides—appear at low levels across all classes but are slightly more prevalent in nontrivial compounds. Halogens, general metals, and noble gases remain minor contributors, consistent with their limited involvement in stabilizing topological electronic structures.

Another feature, the total number of electrons per unit cell (N_e) plays a crucial factor in determining whether a material can exhibit a full band gap or must necessarily be metallic. In closed systems that preserve time-reversal symmetry, Kramers theorem ensures that all electronic bands are at least doubly degenerate.⁶ As a result, systems with odd N_e cannot achieve complete band filling and are thus compelled to be metallic or semimetallic. This theoretical expectation is borne out in our dataset: a substantial 70.7% of TSMs feature odd N_e , reflecting their characteristic gapless nature and partially filled bands.

In contrast, this parity constraint on N_e is less discriminative between trivials and TIs, both of which tend to have even electron counts that allow full band filling. Specifically, 95.7% of trivial compounds and 85.4% of TIs possess even N_e , indicating that electron count alone is insufficient to distinguish trivial from topological phases.

In addition to already described features, we also include bonding characteristics, derived from the total electronegativity difference of constituent elements, as a meaningful compositional descriptor to characterize the chemical bonding nature of materials. This feature is categorized using established thresholds: compounds with an average difference < 0.4 are labeled as very covalent, $0.4\text{--}1.0$ as mostly covalent, $1.0\text{--}2.0$ as moderately ionic, and ≥ 2.0 as highly ionic. This categorization captures the qualitative nature of electron sharing versus transfer, which can significantly affect the emergence of topological phases through orbital hybridization and gap formation. As shown in Table S2, trivial materials tend to be more moderately ionic (58.7%), whereas TIs and TSMs are more frequently mostly covalent (58.8% and 55.4%, respectively), suggesting that increased covalency—often tied to orbital delocalization and band inversion—plays a role in facilitating nontrivial topology. Very covalent bonding is also more prevalent in TIs (14.8%) and TSMs (13.7%) compared to trivial ones (4.9%), further supporting this trend. The low occurrence of highly ionic bonding across all categories (4.0%, 1.7%, and 1.3% for trivials, TIs, and TSMs, respectively) implies that extreme ionicity may be generally unfavorable for topological features, possibly due to the localization of electronic states.

Taken together, this analysis establishes a concise yet physically motivated set of features for characterizing topological materials, including orbital-resolved electron distributions, elemental composition trends, and SG symmetries, as summarized in Table S2. With this foundation, we now proceed to develop and evaluate our approach that leverage these features for predictive classification of materials.

Table S1: SGs with zero probability in each material category.

Trivial	TSM	TI
103, 106, 175, 196, 210, 211	3, 16, 17, 22, 24, 27, 32, 37, 39, 42, 45, 48–50, 77–81, 94, 98, 105, 112, 116, 145, 151, 153, 169, 177, 183, 192, 195, 208	1, 3–9, 16–46, 48, 49, 56, 68, 75–81, 90–92, 94–100, 102–110, 112, 126, 132, 134, 143–146, 149–161, 169, 173–175, 177, 180–183, 185, 186, 188, 192, 195–199, 202, 203, 208, 210–214, 219, 224

S2 Details of the TXL Fusion framework

In this section, we provide a detailed description of each component of the TXL Fusion pipeline.

S2.1 Composition-based heuristic chemical rule module

A framework introduced by Ma et al.⁷ proposes a composition-driven scoring system to assess the likelihood of a material exhibiting specific properties, such as topological behavior. While originally applied to topological materials classification, the approach is general and can be adapted to distinguish any two material categories. In this formulation, each chemical element is assigned a scalar value—referred to as its elemental contribution score (originally termed topogivity, τ_E)—which quantifies its influence on the classification outcome. For a compound M , characterized by the relative abundance $f_E(M)$ of each element E , the overall material score $g(M)$ is computed as a

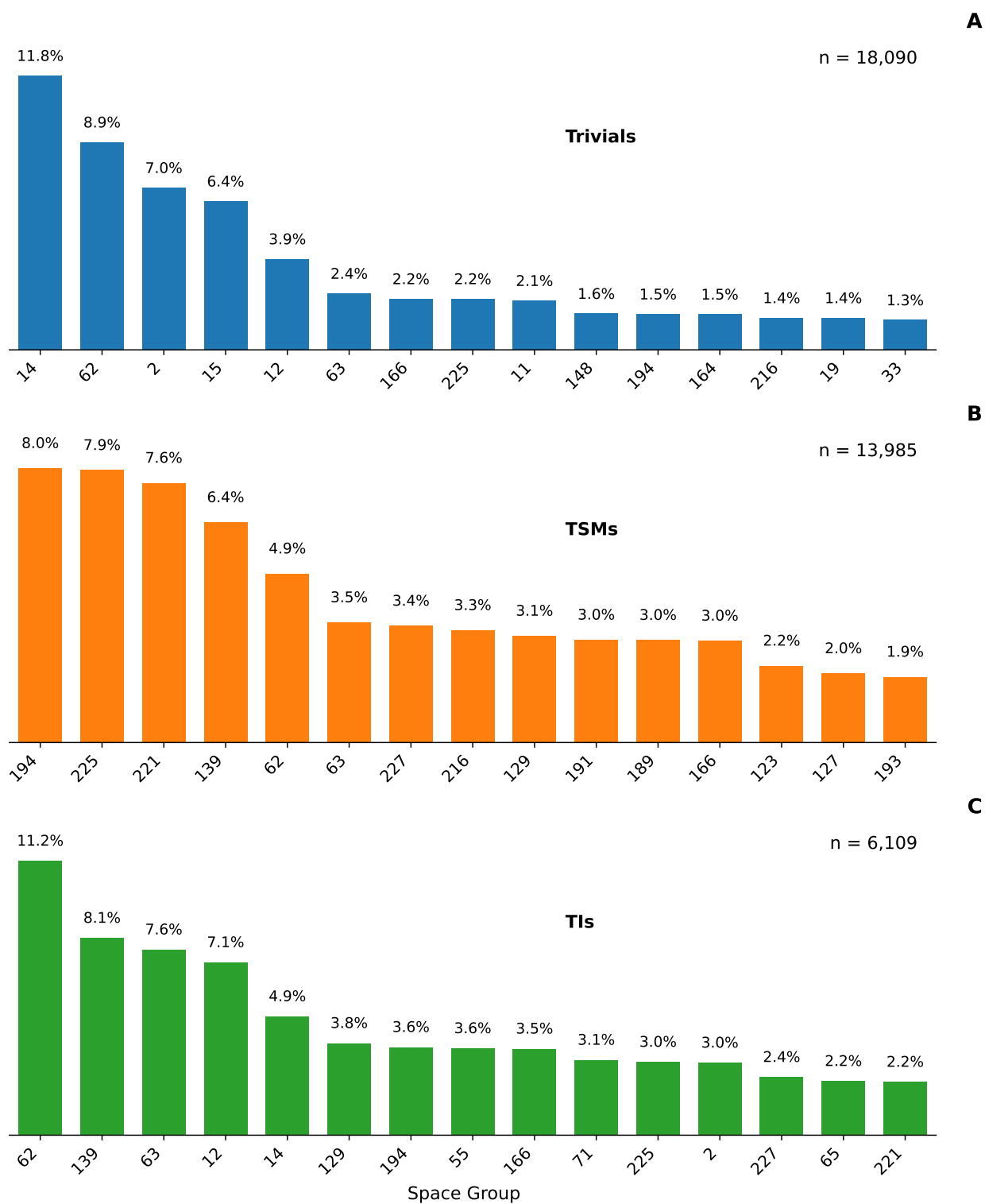


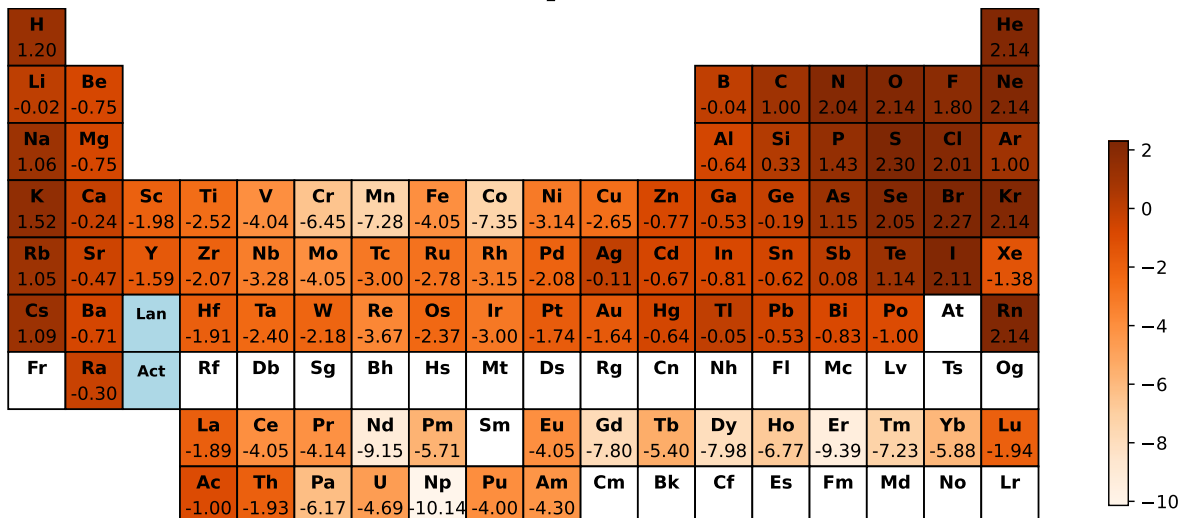
Figure S1: SG distribution of (A) trivial, (B) TSM, and (C) TI compounds where n represents the total number of compounds of a class.

Table S2: Comparative statistical analysis of material classes.

Category	Subcategory	Trivial	TSMs	Topological
Distribution (%)				
	Odd	4.3	70.7	14.6
	Even	95.7	29.3	85.4
Element Ratios (%)				
	Nonmetal	47.4	18.8	21.3
	Halogen	11.9	3.3	2.2
	Transition metal	11.9	36.8	32.8
	Alkali metal	7.9	3.1	2.2
	Metalloid	8.3	11.5	15.9
	Metal	5.4	10.5	9.3
	Alkaline earth metal	4.5	3.6	4.8
	Lanthanide	2.1	10.4	9.6
	Actinide	0.6	1.8	1.9
	Noble gas	0.1	0.1	0.0
Average valence electrons				
	s	1.82	1.80	1.83
	p	2.47	1.20	1.35
	d	0.81	2.48	2.18
	f	0.13	0.80	0.76
d-f valence orbital statistics (%)				
	d & f = 0	42.1	5.0	8.0
	d \neq 0 & f = 0	49.0	58.0	54.0
	d = 0 & f \neq 0	2.0	8.0	7.0
	d & f \neq 0	6.9	29.0	31.0
Bonding Characteristics (%)				
	Very covalent	4.9	14.8	13.7
	Mostly covalent	31.3	54.8	55.4
	Moderately ionic	58.7	26.7	27.8
	Highly ionic	4.0	1.7	1.3

Note: Percentages may not sum to 100% due to rounding.

Element-wise τ_E for trivials



Element-wise τ_E for TSMs

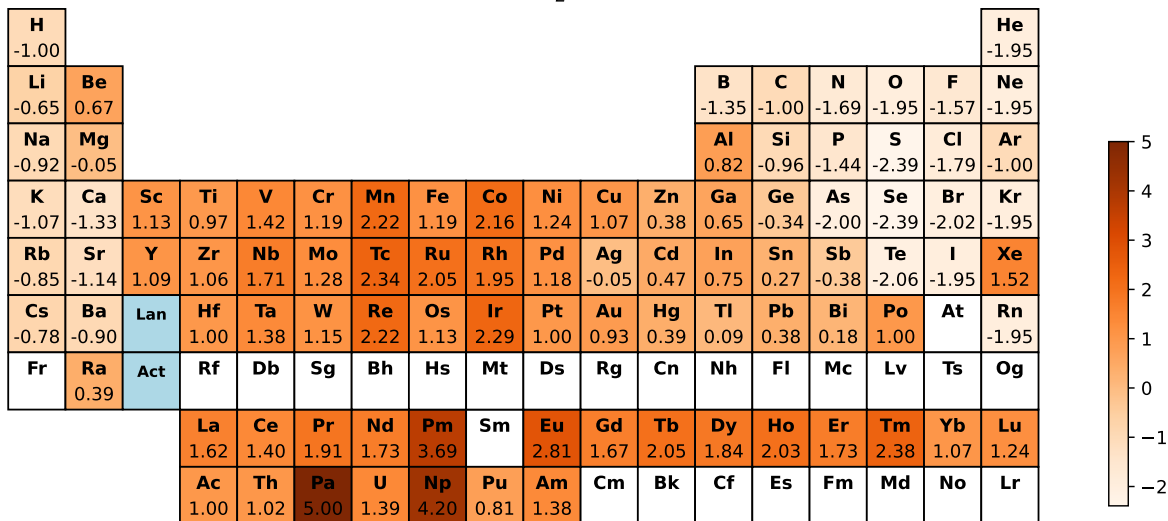


Figure S2: Element-wise τ_E for trivials and TSMs.

weighted sum:

$$g(M) = \sum_E f_E(M)\tau_E. \tag{S1}$$

A higher value of $g(M)$ suggests stronger membership in the positive class (e.g., TI), while a lower (typically negative) score indicates the opposite (e.g., trivial). The elemental scores τ_E are learned by training a linear classifier on a dataset of labeled materials. Each material is first represented as a compositional vector $\tilde{\mathbf{f}}(M)$, which lists the fractional contributions of all elements present (excluding one common element, such as oxygen, to avoid redundancy as it is the most abundant element and can be retrieved using the normalization constraint $\sum_E f_E(M) = 1$). The elements are ordered by increasing atomic number to ensure consistency across the dataset:

$$\tilde{\mathbf{f}}(M) = (f_{\text{Li}}(M), f_{\text{Be}}(M), \dots, f_{\text{U}}(M)). \tag{S2}$$

In our implementation, this results in a 91-dimensional input vector (with 92 different chemical elements in our dataset). The classification task is framed as a binary problem, where one class is labeled as +1, and other classed as -1. A soft-margin linear support vector machine (SVM) is then trained to discriminate between the two categories. The decision function takes the form:

$$Q(M) = \mathbf{w}^T \tilde{\mathbf{f}}(M) + b, \tag{S3}$$

where \mathbf{w} is the weight vector encoding learned elemental contributions and b is a scalar bias. The model is optimized by minimizing a regularized hinge loss:

$$\min_{\mathbf{w}, b} \left[\frac{1}{N} \sum_{i=1}^N \max(0, 1 - y^{(i)}Q(M^{(i)})) + \gamma \|\mathbf{w}\|^2 \right], \tag{S4}$$

where γ is a regularization parameter, $y^{(i)} \in +1, -1$ denotes the class label of material $M^{(i)}$, and N is the total number of training examples. After training, the elemental score for each element is extracted from the learned weights as:

$$\tau_E = \begin{cases} b, & \text{if } E = \tilde{E} \text{ (excluded element)} \\ w_{\iota(E)} + b, & \text{otherwise,} \end{cases} \tag{S5}$$

where $\iota(E)$ maps each element to its corresponding index in the compositional vector $\tilde{\mathbf{f}}(M)$. This simple yet interpretable model captures general chemical trends and provides a compact feature for materials classification. In our study, we extend the binary $g(M)$ chemical rule to a multiclass setting (trivials, TSMs, and TIs), and trained a one-vs-rest linear SVM that assigns an interpretable elemental weight $\tau_E(c)$ for each class c . For any compound M , this yields a three-dimensional score vector

$$\mathbf{g}(M) = [g(M)^{\text{Trivials-Others}}, g(M)^{\text{TSMs-Others}}, g(M)^{\text{TIs-Others}}], \tag{S6}$$

with each component indicating the compound’s alignment with the corresponding class.

Fig. S2 presents periodic table distributions of $\tau_E(c)$ for $g(M)^{\text{Trivials-Others}}$ and $g(M)^{\text{TSMs-Others}}$. The TIs-Others map is omitted here, as it did not successfully distinguish TIs from the other two categories. As can be seen from Fig. S2, the learned weights show clear agreement with known chemical intuition: in the $g(M)^{\text{Trivials-Others}}$ case, alkali metals, nonmetals, halogens, and certain noble gases—elements frequently found in trivial compounds—receive high positive scores. Conversely, in the $g(M)^{\text{TSMs-Others}}$ case, elements with strong SOC such as Bi, Sb, and Te score highly, consistent with their prevalence in TSMs, while lighter elements like H, C, and N receive negative scores, reflecting their association with trivial band structures.

Although Fig. S2 demonstrates the physical interpretability of the $g(M)$ framework, its performance in distinguishing TIs from other compounds especially TSMs is evaluated in the "Results and Discussion" section of the main text, where we have shown that compositional scoring alone is insufficient for this classification.

S2.2 Numerical descriptor module

Unlike composition-based heuristic chemical rule, the numerical descriptor-based framework offers a systematic and transparent classification approach grounded in chemically and physically meaningful features. This methodology encodes each material into a fixed-dimensional vector derived from its elemental composition and structural attributes. The chosen descriptors are designed to capture essential electronic, geometric, and chemical characteristics linked to material behavior.

Let a material M be represented by a descriptor vector $\mathbf{x}(M) \in \mathbb{R}^d$, where each entry corresponds to a specific numerical feature. Based on our features analysis, a key component of $\mathbf{x}(M)$ is the total number of electrons per unit cell, N_e . To capture parity-related effects, we define a binary feature:

$$\delta_{\text{even}}(N_e) = \begin{cases} 1, & \text{if } N_e \pmod{2} = 0 \\ 0, & \text{otherwise} \end{cases} \quad (\text{S7})$$

This feature is a highly predictive indicator for TSMs.

Furthermore, the mean number of valence electrons in each orbital channel (s, p, d, f) is included as:

$$\mu_o(M) = \frac{1}{N_{\text{at}}} \sum_{i=1}^{n_M} N_i \nu_o(E_i), \quad o \in \{\text{s, p, d, f}\} \quad (\text{S8})$$

where n_M is the number of distinct elements in material M , $\nu_o(E_i)$ is the number of valence electrons in orbital o of element E_i , N_i is the number of atoms of element E_i in the formula unit, and $N_{\text{at}} = \sum_i N_i$ is the total number of atoms in M . To indicate whether d- or f-electrons are present in any constituent element, binary flags are included:

$$\delta_d(M) = \max_i \mathbb{I}[\nu_d(E_i) > 0], \quad \delta_f(M) = \max_i \mathbb{I}[\nu_f(E_i) > 0] \quad (\text{S9})$$

which take the value 1 if at least one element in M possesses nonzero d- or f-electron occupancy.

The characteristic of bonding is included via total electronegativity difference of constituent elements. Structural information is incorporated by including the SG number $\text{SG}(M) \in \{1, \dots, 230\}$ as a feature (it is worth mentioning that we only have 216 SGs in our database). In addition, we include conditional probabilities of observing a class $i \in \{\text{trivial}, \text{TI}, \text{TSM}\}$ given the SG g , defined as:

$$P(y = i \mid \text{SG} = g) = \frac{N_i^{(g)}}{N^{(g)}}, \quad (\text{S10})$$

where $N_i^{(g)}$ is the number of materials with SG g and class label i , and $N^{(g)}$ is the total number of materials observed in SG g .

In addition to the raw probabilities, we introduce a derived binary indicator feature that encodes whether the SG is more likely to host class i materials than other classes. This feature is set to 1 if:

$$P(y = i \mid \text{SG} = g) > P(y = \text{other classes} \mid \text{SG} = g), \quad (\text{S11})$$

and 0 otherwise. This formulation enables the model to exploit structural priors learned from the training corpus, capturing class tendencies across crystallographic symmetries.

To incorporate domain knowledge of chemical composition at a higher abstraction level, we also compute category-wise elemental fractions. Each element is assigned to a chemically meaningful category based on its position in the periodic table—such as alkali metals, alkaline earth metals, transition metals, halogens, nonmetals, metalloids, lanthanides, actinides, and others. For a material M , the fraction of atoms belonging to category $c \in \mathcal{C}$ is defined as:

$$\phi_c(M) = \sum_{E \in M} f_E(M) \mathbb{I}[E \in c], \quad (\text{S12})$$

where $f_E(M)$ is the fractional composition of element E and $\mathbb{I}[E \in c]$ is an indicator function equal to 1 if element E belongs to category c , and 0 otherwise. The resulting fixed-length vector $(\phi_c(M))_{c \in \mathcal{C}}$ encodes the distribution of atoms across elemental families, allowing the model to generalize across broad compositional trends that correlate with topological behavior. All features, including symmetry-based statistics, electronic structure features, and compositional summaries, are concatenated into a single feature vector $\mathbf{x}(M)$.

S2.3 LLM: Semantic descriptor based module

The motivation for employing LLMs in material detection lies in their capacity to unify structured data with contextual domain knowledge into a cohesive, high-dimensional representation. Unlike conventional numerical descriptors that factorize material properties into isolated scalars, LLM embeddings utilize self-attention mechanisms to capture coupled physical effects—such as the intricate interplay between crystalline symmetry and SOC—as unified, context-aware vectors.

By leveraging models like SciBERT, which are pretrained on extensive scientific corpora, these embeddings inherit latent physical regularities and established domain heuristics. This enables the classification pipeline to exploit complex, non-linear correlations between orbital character and

band topology that are often inaccessible through traditional, hand-crafted features, ultimately facilitating more robust and physically-informed material discovery. A comparative discussion of semantic and numerical descriptors is provided in Section S4.

To implement this, each compound is encoded into a structured narrative that reflects domain-relevant priors and inter-feature dependencies. Specifically, the template includes the chemical formula, SG designation (with an explanatory note on how symmetry influences band topology), and element category ratios to reflect chemical diversity. It further includes average valence electron contributions by orbital type, emphasizing d/f-electron content which often correlates with nontrivial topology. Total valence and total electron counts are included with parity annotations, capturing heuristic cues associated with topological phases. Precomputed class probabilities (trivials, TSMs, TIs) for the corresponding SG are also embedded, along with composition-based heuristic chemical rules $g(M)$ for trivials and TSMs.

To enhance transparency and model interpretability, we incorporate conditional heuristic rules into the narrative. For example, when a class (e.g., trivial, TSM or TI) has zero probability under the symmetry group prediction (Table S1), we append a rationale grounded in the direction (positive/negative) of the composition-based scores. Similar logic is applied even when all class probabilities are non-zero, providing additional interpretive cues. These cases are explicitly marked as "heuristic predictions (not guaranteed)" to differentiate them from purely model-derived outputs.

We utilize the `scibert_scivocab_uncased` model⁸ for its specialization in scientific text, pretrained on 1.14 million scholarly articles using a domain-tailored vocabulary. Its lightweight architecture (110M parameters) ensures efficient fine-tuning while maintaining strong semantic capabilities for scientific reasoning tasks. The training details can be found in the following section.

S3 Training details

This section provides a comprehensive description of the training procedures for all models employed in this study, including the composition-based heuristic, standalone XGBoost (XGB) model, and the TXL Fusion framework. Each subsection details feature preparation, model configuration, hyperparameter selection, and training strategies.

S3.1 Composition-based heuristic chemical rule

In the case of $g(M)$ composition-based heuristic chemical rule, we train a support vector machine (SVM) model using a dataset where each compound was represented by its chemical formula, which was transformed into feature vector $\mathbf{f}(M)$ encoding the relative atomic fractions of elements present in the compound, excluding oxygen. The elemental composition was standardized using the `pymatgen` library to ensure consistent parsing of formulas, and the feature space was constructed using the normalized fractions of all non-oxygen elements across the dataset, resulting in a fixed-dimensional input vector for each compound. Labels were assigned as +1 for the concerned class and -1 for other classes after mapping the original classification labels to this binary scheme. The SVM model employed a linear kernel and was regularized using a soft margin, where the regularization parameter C was set as the inverse of the product of the number of training samples and a predefined gamma value ($\gamma=1.28e-6$), effectively linking the penalty term to the scale of the data. The model

was trained on the full prepared dataset without an explicit validation split during training, fitting the decision boundary to maximize the margin between the two classes while allowing for some misclassification through the soft margin.

S3.2 Standalone XGB model

The standalone XGB classifier was trained using a stratified train-validation split with 80% of the data used for training and 20% reserved for validation (`random_state = 42` to ensure reproducibility). The multi-class labels—trivial, TSM, and TI—were encoded using a `LabelEncoder` and mapped to integer values to facilitate model training. The model was configured with a moderate maximum depth of 4 to control complexity and reduce overfitting, a low learning rate of 0.01, and an increased number of estimators (1,000). Early stopping was implemented with a patience of 20 rounds based on validation performance. Regularization was enforced through L1 (`reg_alpha = 0.2`) and L2 (`reg_lambda = 2.0`) penalties, along with gamma pruning (`gamma = 0.2`) to discourage insignificant splits. Additional robustness was achieved via subsampling (70% of samples and features per tree, controlled by `subsample = 0.7` and `colsample_bytree = 0.7`) and a minimum child weight of 3 to avoid overfitting to small partitions. Training was accelerated using GPU computation (`device = 'cuda', tree_method = 'hist'`) and evaluated on the validation set using multi-class log loss (`eval_metric = 'mlogloss'`). After training, the best-performing model was saved in JSON format for reproducibility, and predictions on the validation set were used to compute a detailed classification report, including precision, recall, and F1-score per class.

S3.3 Finetuning of LLM for TXL Fusion

The semantic component of TXL Fusion is provided by a fine-tuned LLM, `scibert_scivocab_uncased`, chosen for its domain relevance in scientific literature. The base model contains 110M parameters with a 768-dimensional hidden size and 12 attention heads. A lightweight classification head was appended, and the entire model—including embedding layers—was fine-tuned using the Hugging Face Trainer API with the AdamW optimizer (learning rate $2e-5$, batch size 16 per device) for 8 epochs. Input narratives were padded or truncated to 512 tokens, and the self-attention mechanism enabled the model to capture contextual relationships among features such as SG symmetry, orbital occupancy, and electron parity. The resulting embeddings encode higher-order interactions that complement the hand-engineered descriptors. To improve computational efficiency and reduce redundancy, the 768-dimensional embeddings were compressed via principal component analysis (PCA) to 5 dimensions.

S3.4 Training of TXL Fusion

The TXL Fusion model was trained on a unified feature set integrating information from three sources: the composition-based heuristic, the numerical descriptors used in the standalone XGB model, and fine-tuned LLM embeddings. Specifically, the feature set includes the heuristic scores $g(M)^{\text{Trivial-Others}}$ and $g(M)^{\text{TSM-Others}}$, together with binary flags indicating whether each score is positive, exceeds 1.0, or falls below -1.0. These features were concatenated with the PCA-reduced LLM embeddings and the numerical descriptors to form a comprehensive input vector. The dataset

was split 80–20 using stratified sampling to preserve class balance across trivial, TSM, and TI categories (`random_state=42`). The XGBoost classifier was trained on this concatenated feature space with the same hyperparameters as the standalone XGB model, ensuring a consistent and comparable evaluation.

S4 Semantic versus numerical descriptor: performance comparison

Conventional numerical descriptors encode materials using explicit, hand-crafted features such as SG, total electron count, orbital occupations, elemental ratios, and heuristic topology indicators. While physically interpretable, these descriptors are intrinsically factorized, treating each quantity as an independent variable. Consequently, coupled physical effects—such as the interplay between crystal symmetry, orbital character, and electron filling that governs band inversion and symmetry-protected states—are not explicitly represented and must instead be inferred indirectly through nonlinear models or additional feature engineering.

Semantic descriptors provide an alternative by embedding expert knowledge and physical heuristics directly within a natural-language representation. Fig. S3 illustrates this contrast for $\text{Ce}_1\text{K}_2\text{O}_{15}\text{Si}_6$ (SG 15). The semantic descriptor integrates compositional ratios, orbital-resolved valence electron information, symmetry context, and qualitative physical reasoning into a single narrative input. This formulation allows conditional expert insights—such as the relationship between d/f-electron contributions and topological behavior, or the interpretive role of electron parity—to be encoded contextually, without discretization into binary flags or threshold-based rules. When processed by a LLM, the semantic descriptor is mapped to a context-aware embedding in which data-driven features and domain knowledge are implicitly fused. In contrast, the numerical descriptor represents the same information as a high-dimensional vector of isolated scalar features, including orbital-presence indicators, electron-parity flags, and thresholded topogivity scores. Although both representations yield a trivial classification for this compound, the semantic descriptor preserves physical relationships that are fragmented across independent dimensions in the numerical representation.

The effectiveness of semantic descriptors is further enhanced by transfer learning. Models such as SciBERT are pretrained on large scientific corpora spanning condensed matter physics and materials science, resulting in embedding spaces shaped by established physical regularities, including correlations between heavy elements and strong SOC coupling, specific SGs and symmetry-protected degeneracies, and orbital character and band topology. As a result, the generated embeddings reflect not only the provided input information but also accumulated domain knowledge embedded during pretraining.

Self-attention mechanisms also play a central role in capturing these relationships by conditioning the representation of one concept on the simultaneous presence of others. For example, elemental identity is embedded jointly with symmetry context, enabling the representation to encode the potential for symmetry-protected band crossings and SOC-driven band inversion prior to classification—relationships that are not explicitly accessible in conventional numerical feature spaces.

The enhanced physical expressiveness of these representations is reflected in the geometry of the LLM embedding space derived from the semantic descriptors. As shown in Fig. S4, UMAP projections of numerical descriptors exhibit weak phase separation, with silhouette scores of 0.0414

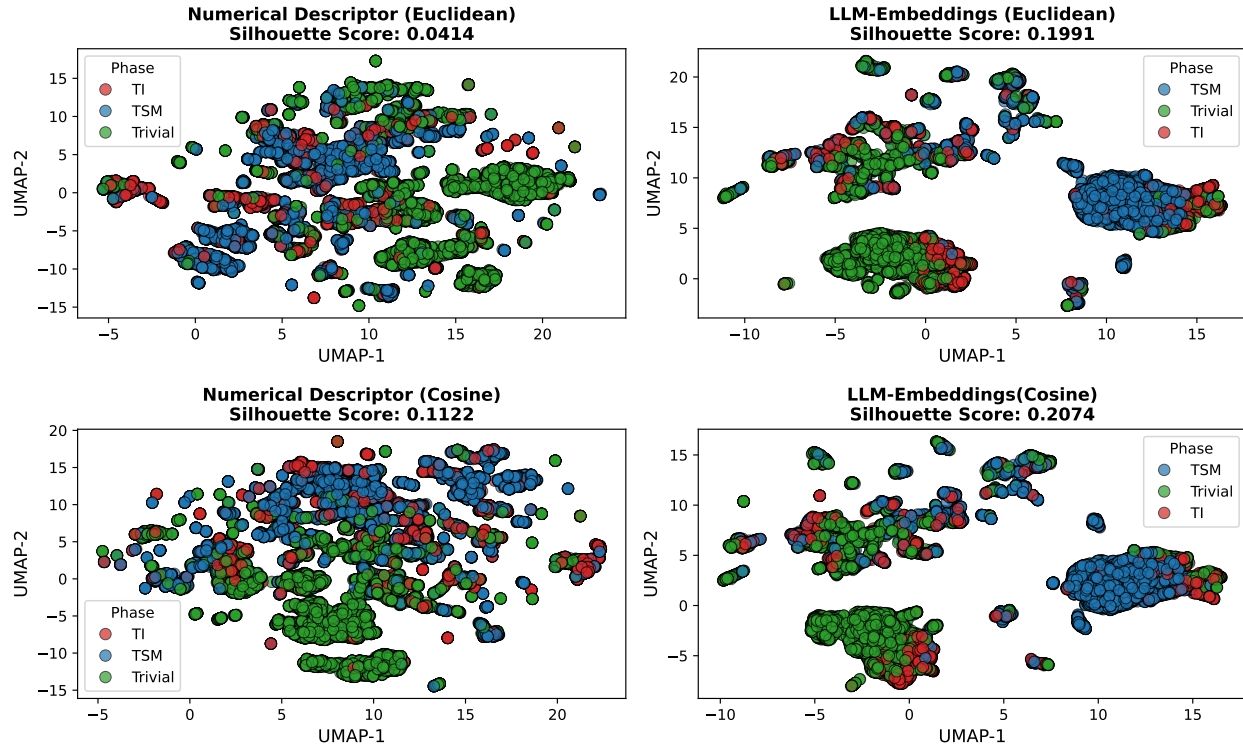
LLM Semantic Descriptor

Your task is to classify this compound as 'trivial', semimetal or 'topological'.
Compound: Ce₁K₂O₁₅Si₆. Space group: 15. Note: Changes in space group can influence band topology and shift a material between trivial and topological phases. Ratio of elements (%): {'alkali metal': '8.33', 'alkaline earth metal': '0.00', 'nonmetal': '62.50', 'halogen': '0.00', 'noble gas': '0.00', 'transition metal': '0.00', 'metal': '0.00', 'lanthanide': '4.17', 'actinide': '0.00', 'metalloid': '25.00'} Mean valence electrons by orbital type: {'s': 1.92, 'p': 3.0, 'd': 0.04, 'f': 0.04} (high value of d and f electrons often correlates with semimetal and topological behavior). Total electrons: 300.0 (even) (odd numbers often indicate semimetallic nature). Probabilities for the space group: 78.26% trivial, 13.50% semimetal, 8.24% topological. Topogivity score for the compound to be trivial: 1.38 (positive value suggests trivial nature of the compound). Topogivity score for the compound to be semimetal: -1.49 (positive value suggests semimetallic nature of the compound). Based on these features, determine the correct classification. Heuristic prediction (not guaranteed): Topogivity score for the compound to be trivial is positive, and the topogivity score for the compound to be semimetal is negative, thus we predict this compound is likely trivial.

Numerical Descriptor

```
"SG": 15, "Total_electrons": 300.0, "Trivial_g(M)": 1.38,
"Is_trivial_g(M)_positive?": 1, "Is_trivial_g(M)_gt_than_1?": 1,
"Is_trivial_g(M)_sl_than_minus_1?": 0, "SM_g(M)": -1.49, "Is_SM_g(M)_positive?": 0,
"Is_SM_g(M)_gt_than_1?": 0, "Is_SM_g(M)_sl_than_minus_1?": 1, "Mean_s_valence_electrons":
1.92, "Mean_p_valence_electrons": 3.0, "Mean_d_valence_electrons":
0.04, "Mean_f_valence_electrons": 0.04, "Is_d_val_electrons_present?": 1,
"Is_f_val_electrons_present?": 1, "Is_total_electrons_even?": 1, "Trivial_SG_prob":
0.7826, "SM_SG_prob": 0.1350, "TI_SG_prob": 0.0824, "Trivial_vs_others_SG_prob":
1, "SM_vs_others_SG_prob": 0, "TI_vs_others_SG_prob": 0, "label": "trivial",
"Alkali_metal": 8.33, "Alkaline_earth_metal": 0.0, "Nonmetal": 62.50, "Halogen":
0.0, "Noble_gas": 0.0, "Transition_metal": 0.0, "Metal": 0.0, "Lanthanide":
4.17, "Actinide": 0.0, "Metalloid": 25.0
```

Figure S3: Comparative representation of material descriptors for Ce₁K₂O₁₅Si₆ (SG 15). The Semantic Descriptor (Top) leverages natural language to embed domain-specific heuristics and physical context, whereas the Numerical Descriptor (Bottom) represents the same data as a collection of isolated, high-dimensional feature vectors.



(Euclidean) and 0.1122 (cosine), indicating substantial overlap between trivial, semimetallic, and topological phases. In contrast, UMAP projections constructed from fine-tuned SciBERT embeddings show markedly improved clustering, with silhouette scores increasing to 0.1991 (Euclidean) and 0.2074 (cosine).

The consistency of this improvement across distance metrics indicates that the enhanced separability arises from the intrinsic geometry of the learned embedding space rather than from the choice of similarity measure. Overall, semantic descriptors, when mapped to LLM embeddings, complement conventional numerical features by capturing context-dependent electronic–structural correlations that are difficult to encode in factorized numerical form, enabling more reliable discrimination of subtle topological regimes.

S5 Element-resolved performance and confidence analysis

In this section, we present an analysis of our models’ behavior as a function of both the number of constituent elements and the associated prediction confidence, providing complementary insights into accuracy, robustness, and calibration across different chemical regimes.

Performance trends with respect to chemical complexity are summarized in Tables S3 and S4, which report class-wise precision, recall, F1-score, and support for the numerical descriptor-based XGB model and the TXL Fusion model, respectively. For single-element compounds, both models exhibit limited predictive capability for TI phases, with F1-scores below 0.25, reflecting the intrinsic difficulty of resolving topology in chemically simple systems. Performance improves for two- and three-element compounds, where TXL consistently outperforms XGB, achieving F1-scores of approximately 0.62–0.64 compared to 0.59–0.63 for XGB.

The largest performance differences emerge for four- and five-element compounds. In this regime, TXL sustains stable and reliable predictions for TIs ($F1 = 0.57$ and 0.61), whereas XGB performance drops sharply ($F1 = 0.24$ and 0.31), reflecting a diminished ability to capture subtle topological signatures. For six-element systems, both models perform well on trivial and TSM classes; however, TXL maintains better balance for the relatively scarce TI class, achieving an F1-score of 0.33 compared to 0.00 for XGB. These results highlight that the advantage of the TXL fusion architecture grows with increasing chemical and electronic complexity.

Prediction reliability is further examined through confidence-based calibration analysis, shown in Fig. S5. The TXL Fusion model exhibits strong calibration at high confidence levels: predictions exceeding 90% confidence are nearly always correct across all classes and are supported by sufficient sample counts. In contrast, predictions in the intermediate confidence range (30–50%) are less reliable, with observed accuracies frequently falling below the midpoint of the corresponding bins, indicating residual overconfidence. This effect is most evident in the 30–40% confidence range, where trivial-class predictions achieve perfect accuracy but are based on only three samples, rendering the apparent performance statistically insignificant.

S5.1 Origins of reduced performance in low-complexity compounds

Table S3: Classification performance of the numerical descriptor-based XGB model for compounds grouped by the number of constituent elements (1–6). Precision, recall, F1-score, and support (number of samples) are reported for the trivial, TSM, and TI classes.

Elements	Class	Precision	Recall	F1-score	Support
1-Element Compounds (n = 108)					
	Trivial	0.75	0.79	0.77	34.0
	TSM	0.70	0.76	0.73	50.0
	TI	0.27	0.20	0.24	24.0
2-Element Compounds (n = 1,835)					
	Trivial	0.74	0.76	0.75	545.0
	TSM	0.82	0.89	0.85	901.0
	TI	0.68	0.51	0.59	389.0
3-Element Compounds (n = 3,749)					
	Trivial	0.88	0.88	0.88	1612.0
	TSM	0.83	0.89	0.86	1439.0
	TI	0.69	0.58	0.63	698.0
4-Element Compounds (n = 1,524)					
	Trivial	0.89	0.97	0.93	1073.0
	TSM	0.80	0.82	0.81	292.0
	TI	0.54	0.15	0.24	159.0
5-Element Compounds (n = 354)					
	Trivial	0.96	0.97	0.97	284.0
	TSM	0.90	0.93	0.91	57.0
	TI	0.50	0.23	0.31	13.0
6-Element Compounds (n = 67)					
	Trivial	0.96	0.94	0.95	53.0
	TSM	0.73	1.0000	0.85	11.0
	TI	0.0000	0.0000	0.0000	3.0

Table S4: Classification performance of the TXL Fusion model for compounds grouped by the number of constituent elements (1–6). Precision, recall, F1-score, and support (number of samples) are reported for the trivial, TSM, and TI classes.

Elements	Class	Precision	Recall	F1-score	Support
1-Element Compounds (n = 108)					
	Trivial	0.77	0.79	0.78	34.0
	TSM	0.68	0.84	0.76	50.0
	TI	0.33	0.17	0.22	24.0
2-Element Compounds (n = 1,835)					
	Trivial	0.77	0.76	0.77	545.0
	TSM	0.82	0.89	0.86	901.0
	TI	0.69	0.57	0.62	389.0
3-Element Compounds (n = 3,749)					
	Trivial	0.87	0.91	0.89	1612.0
	TSM	0.87	0.86	0.87	1439.0
	TI	0.68	0.61	0.64	698.0
4-Element Compounds (n = 1,524)					
	Trivial	0.92	0.96	0.94	1073.0
	TSM	0.88	0.81	0.84	292.0
	TI	0.62	0.53	0.57	159.0
5-Element Compounds (n = 354)					
	Trivial	0.97	0.97	0.97	284.0
	TSM	0.89	0.88	0.88	57.0
	TI	0.61	0.61	0.61	13.0
6-Element Compounds (n = 67)					
	Trivial	0.96	0.96	0.96	53.0
	TSM	1.00	1.00	1.00	11.0
	TI	0.33	0.33	0.33	3.0

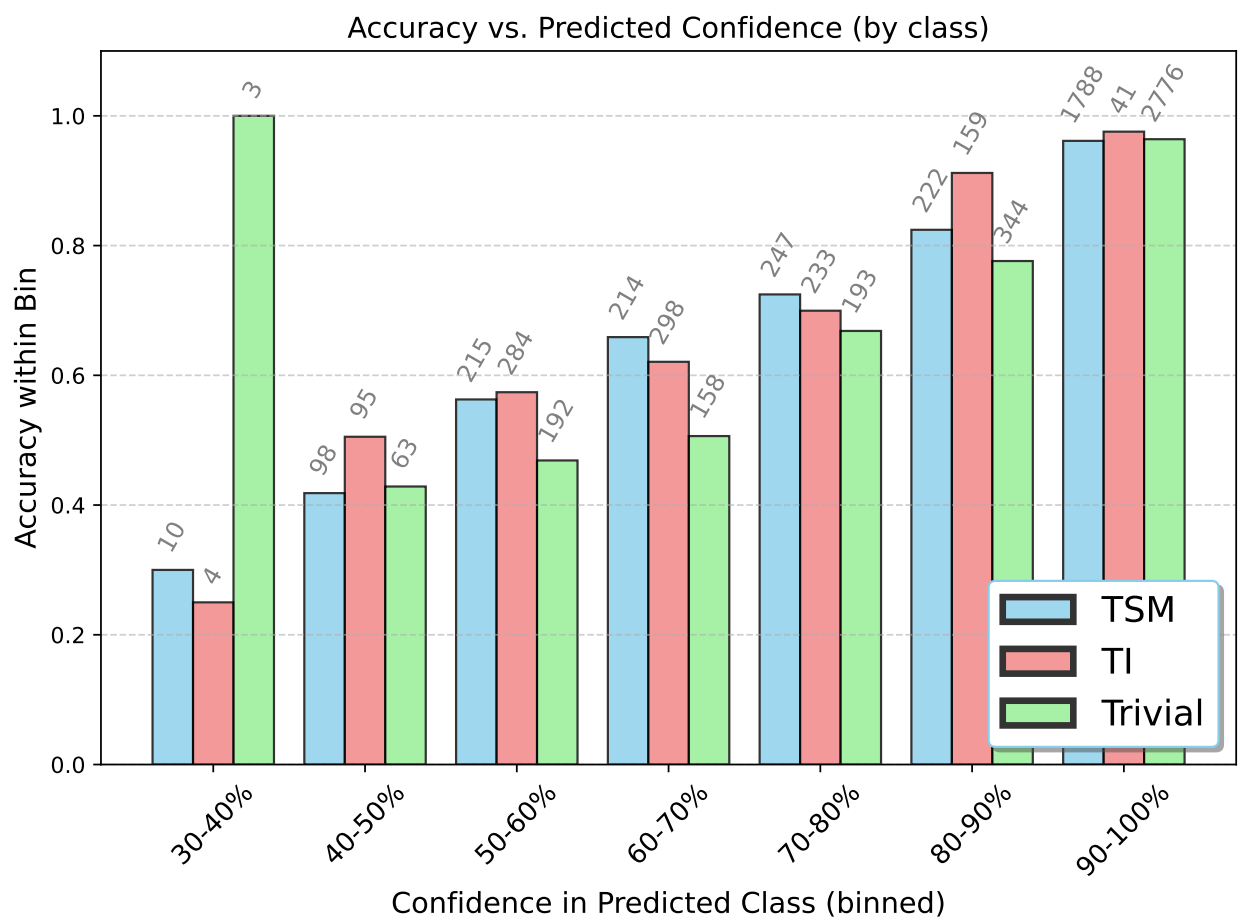


Figure S5: Accuracy versus predicted confidence for each class (TSM, TI, trivial), binned by the TXL Fusion’s confidence in its predicted class. Each bar represents the accuracy within a confidence bin (e.g., 0.3–0.4), with height indicating the fraction of correctly classified samples in that bin. The number atop each bar shows the sample count. The plot reveals how well the model’s confidence aligns with its actual accuracy per class.

Distribution of Materials by Number of Constituent Elements

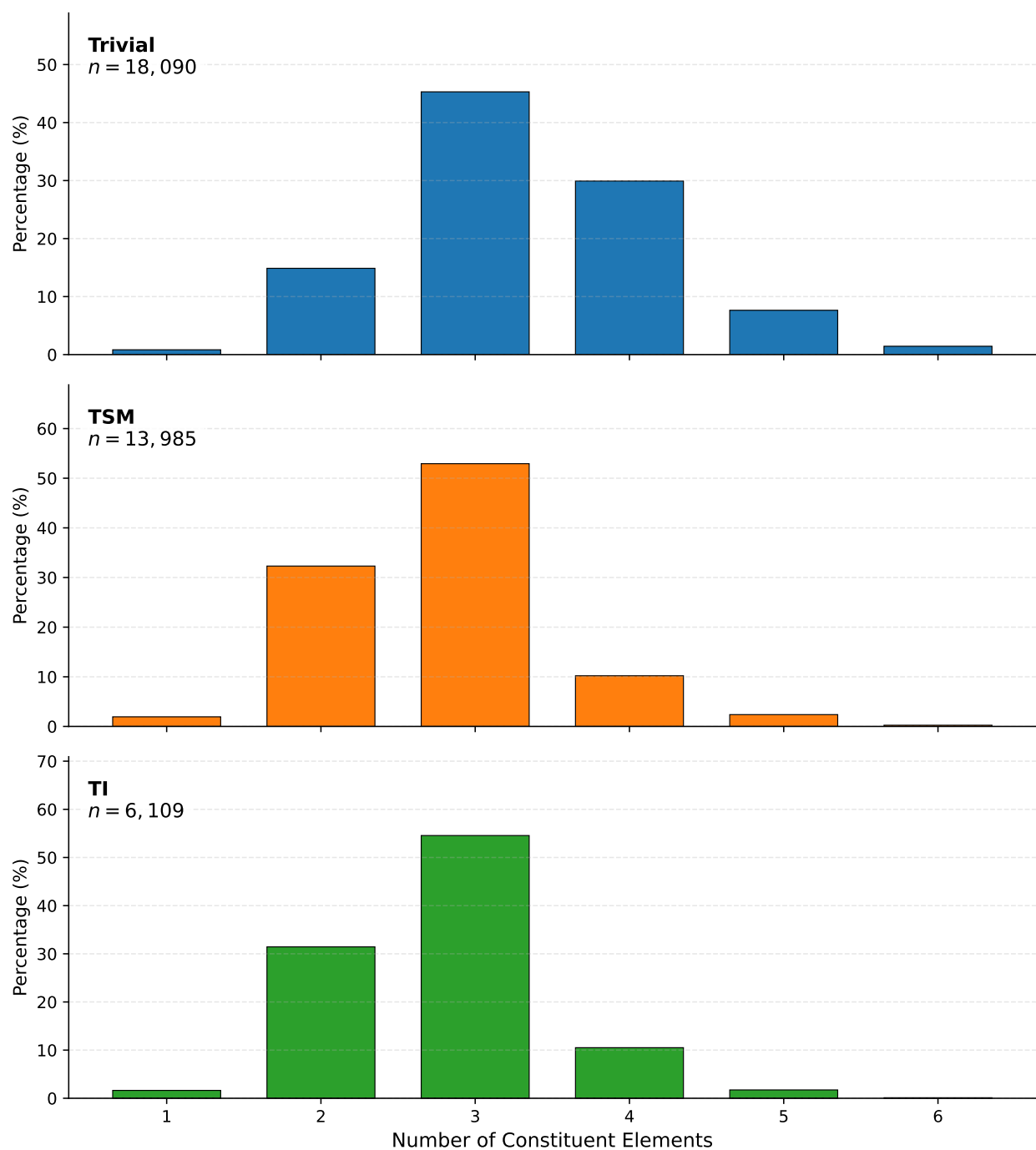


Figure S6: Histogram of dataset composition (%). Across all classes, the dataset is dominated by ternary compounds, with quaternary systems forming the next largest group. Binary materials contribute a substantial fraction for TSMs and TIs but are less prevalent for trivial phases. In contrast, single-element compounds and high-entropy materials with five or six elements are strongly underrepresented, particularly for TIs, reflecting pronounced data sparsity in these chemical regimes.

The reduced performance observed for single- and binary-element compounds, as reported in Tables S3 and S4, arises from inherent limitations in the data, the descriptors, and the underlying physics of these systems.

First, data scarcity constrains learning in low-complexity regimes. As shown in Fig. S6, single-element compounds account for only a very small fraction of the labeled dataset across all classes, while binary compounds—although more prevalent, particularly for TSM and TI—still represent a limited compositional space compared with ternary systems that dominate the data. This uneven coverage reduces statistical diversity for low-complexity materials and leads to less well-constrained decision boundaries in these regimes.

Second, composition-based descriptors further amplify this challenge. Many features—such as elemental category ratios, electronegativity contrasts, and multi-orbital interaction proxies—rely on comparisons across distinct atomic species. In single-element systems, these features collapse to constants or vanish, and in binary compounds they span a narrow range, limiting their discriminative power. By contrast, compositionally complex materials provide richer chemical and structural diversity, allowing numerical descriptors and language-model embeddings to capture high-dimensional, distinctive patterns that encode coupled electronic–structural effects. As shown in the element-resolved performance analysis summarized in Table S4, despite their scarcity, five- and six-element materials achieve substantially better TXL Fusion performance than single- and binary-element compounds.

Third, the underlying physics of low-complexity compounds is often governed by subtle, non-compositional factors. Topological phase transitions in these systems depend sensitively on precise lattice parameters, symmetry-breaking distortions, strain-modulated SOC, and fine details of band inversion near the Fermi level. While our compositional descriptors are highly effective at capturing broad trends across vast chemical spaces, they are inherently limited in their ability to resolve such microscopic, quantum-mechanical details. This fundamental mismatch between descriptor resolution and the physical mechanisms at play further constrains predictive accuracy for chemically simple materials.

However, these limitations can be mitigated by incorporating more localized or symmetry-resolved physical descriptors, such as symmetry-indicator eigenvalues, band inversion indicators, Wannier charge centers, or orbital-projected band-edge features. These features better capture the physics underlying low-complexity topological materials but are computationally intensive and not uniformly available at scale. Within our framework, we prioritize broad chemical coverage, detecting material classes based solely on elemental properties without requiring features that need prior expensive calculations.

S5.2 Generalization of TXL Fusion under chemical sparsity

To evaluate the generalization capability of TXL Fusion in sparsely sampled chemical regimes, we analyze its performance as a function of elemental complexity. As shown in Fig. S6, single-, five-, and six-element compounds are strongly underrepresented in the topological materials database⁴ (used in our work for training) and can therefore be regarded as sparsely sampled or partially out-of-distribution. Within their respective class distributions, these regimes account for trivial (0.83%, 7.64%, 1.44%), TSM (1.94%, 2.38%, 0.24%), and TI (1.64%, 1.74%, 0.11%) compounds. Because five-element trivial compounds are comparatively less sparse (7.64%), they are excluded from the

sparsity-focused discussion below.

As shown in Table S4, for trivial compounds, TXL Fusion maintains strong predictive performance despite extreme sparsity in the single- and six-element regimes ($\approx 0.8\%$ and 1.4%), achieving F1-scores of 0.78 and 0.97, respectively. The lower performance for single-element compounds and the improved performance in higher-element systems are discussed in the preceding Section S5.1.

For TSMs, F1-scores increase from 0.75 for single-element systems to 0.84 for five-element systems and reach 1.00 for six-element systems, though the latter is based on limited support (11–57 samples). This trend indicates that even in sparse regimes, increasing combinatorial diversity provides patterns that the model can effectively leverage.

In contrast, TIs remain the most challenging class. Beyond their overall underrepresentation in the whole dataset (16%), extreme sparsity in the single- and six-element regimes—particularly six-element compounds (0.11%)—yields substantially reduced performance (F1 = 0.22 and 0.33). Moderate recovery is observed for five-element TIs (F1 = 0.62), based on only 13 samples. These results reflect both severe data scarcity and the subtle, non-compositional physics that govern TI phases.

Overall, these results indicate that TXL Fusion maintains reliable predictive capability for trivial and TSM phases even in sparsely sampled chemical families. In contrast, performance for TI phases is primarily constrained by intrinsic data scarcity, suggesting that further improvements are likely as additional labeled TI data become available.

S6 DFT computational details

DFT calculations were carried out using the VASP package.^{9,10} The core and valence electrons are considered within the projector augmented wave method by taking a cutoff of 600 eV for the plane wave basis.¹¹ For structural optimization, both the volume and atomic position relaxations are performed until the force and energy differences were less than 0.001 eV/Å and 10–8 eV, respectively. An appropriate k-mesh was chosen for each structure depending on the lattice parameters. All the electronic band structure calculations were performed by considering the SOC effects.

S7 Reliability of DFT-based topological labels and implications for training

As noted in the concluding remarks of the main text, one factor limiting the predictive performance of TXL Fusion is the intrinsic noise present in the DFT-based labels used for training. Although first-principles calculations form the backbone of large-scale topological materials databases, their reliability is not uniform across chemical space. In particular, the topological materials database employed in this work explicitly cautions against fully trusting ab initio predictions for more than 2300 compounds containing partially filled *f*-electron shells, where standard DFT approximations are challenged by strong correlation effects and complex band structures (see SI Appendix M of Ref. 4).

Beyond *f*-electron systems, the database authors further recommend performing Wilson-loop cal-

culations for all materials in order to robustly validate the predicted topological invariants. In addition, for materials containing partially filled d or f shells, the authors explicitly recommend re-examining these systems using more accurate many-body approaches such as dynamical mean-field theory (DMFT), which properly accounts for electronic correlation effects beyond standard DFT.

Even outside strongly correlated regimes, DFT-derived topological labels remain particularly fragile for small-gap or borderline materials. In such cases, band inversions and symmetry-protected features can be highly sensitive to numerical details, including the choice of exchange–correlation functional, spin–orbit coupling strength, and k -point sampling. Consequently, even minor computational variations may alter the predicted topological classification, introducing unavoidable label ambiguity. Such ambiguity effectively manifests as label noise, rendering certain compounds intrinsically difficult—or even impossible—to predict reliably within a supervised learning framework.

To evaluate the impact of label noise on model performance, we test the hypothesis that TXL Fusion performs more robustly on high-confidence subsets of the data. Specifically, we construct two High-Confidence Material (HCM) subsets from Discovery Space–1 by selecting TIs with relatively large direct gaps, for which DFT-based classifications are expected to be more reliable. The first subset (HCM-1) comprises 419 TI compounds with direct gaps exceeding 0.035 eV, while the second, more stringent subset (HCM-2) contains 356 TI compounds with direct gaps larger than 0.045 eV.

When evaluated exclusively on these HCM datasets, TXL Fusion exhibits systematically improved classification performance for the TI class. As shown in Fig. S7, for the HCM-1 dataset, the model achieves a precision of 0.68, a recall of 0.54, and an F1 score of 0.60. For the higher-confidence HCM-2 dataset, precision further increases to 0.76, with a recall of 0.52 and an F1 score of 0.62. The monotonic improvement in precision and F1 score with increasingly stringent confidence criteria supports the interpretation that label noise in small-gap and borderline systems significantly suppresses apparent model performance in the full dataset.

These results indicate that a non-negligible fraction of misclassifications arises not from limitations of the learning architecture itself, but from uncertainties inherent to the underlying DFT labels. This observation underscores an important practical consideration for data-driven topological materials discovery: gains in model accuracy are fundamentally constrained by the fidelity of reference labels, highlighting the critical need for highly reliable and systematically validated topological materials databases.

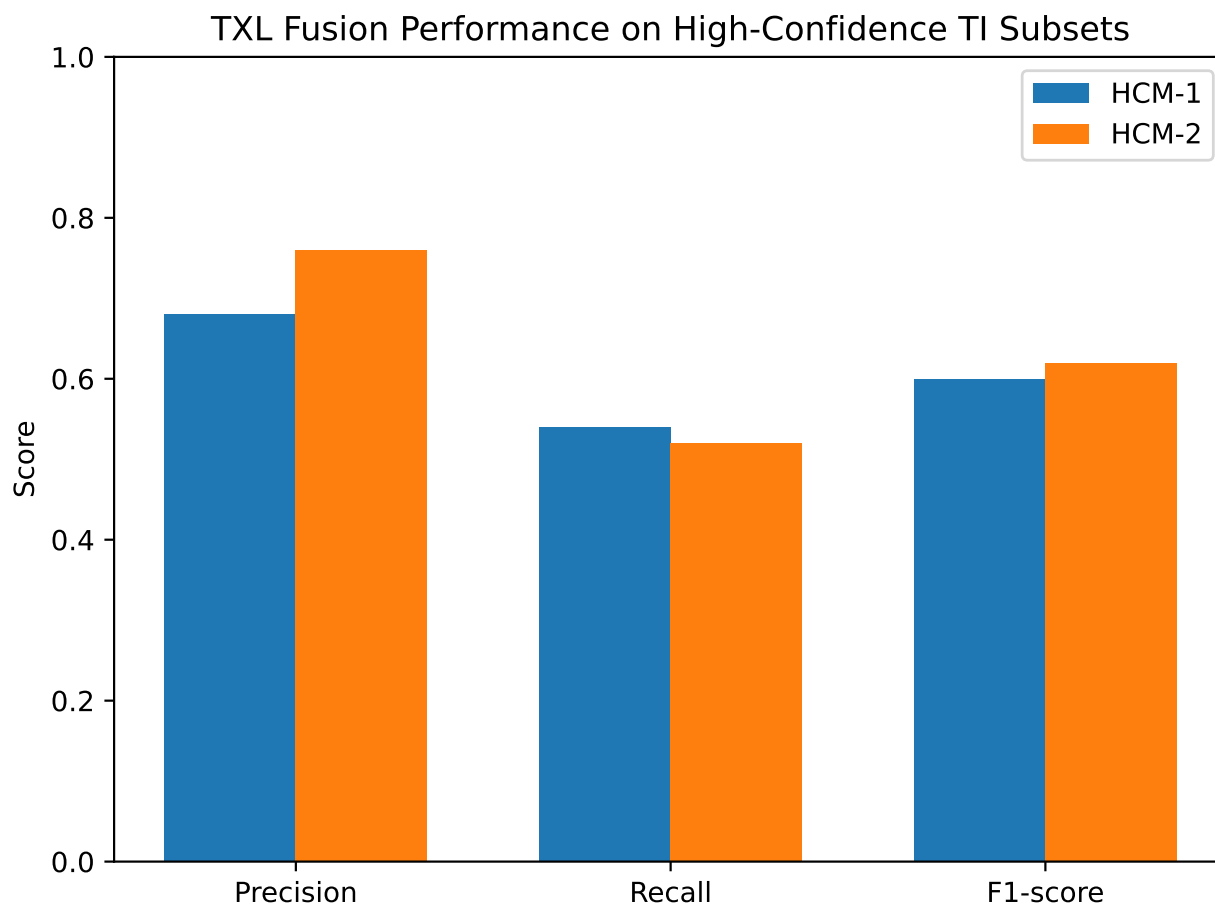


Figure S7: Performance of TXL Fusion on high-confidence TI subsets. Precision, recall, and F1-score are reported for two HCM datasets derived from Discovery Space-1. HCM-1 includes TI compounds with direct gaps exceeding 0.035 eV, while HCM-2 applies a stricter threshold of 0.045 eV. The monotonic improvement in precision and F1-score for HCM-2 highlights the impact of label noise in small-gap and borderline systems on apparent model performance.

References

- [1] Topological Materials Database. <https://www.topologicalquantumchemistry.org/#/>.
- [2] Bilbao Crystallographic Server. <https://www.cryst.ehu.es/>.
- [3] Bradlyn, B.; Elcoro, L.; Cano, J.; Vergniory, M. G.; Wang, Z.; Felser, C.; Aroyo, M. I.; Bernevig, B. A. Topological quantum chemistry. *Nature* **2017**, *547*, 298–305.
- [4] Vergniory, M.; Elcoro, L.; Felser, C.; Regnault, N.; Bernevig, B. A.; Wang, Z. A complete catalogue of high-quality topological materials. *Nature* **2019**, *566*, 480–485.
- [5] Vergniory, M. G.; Wieder, B. J.; Elcoro, L.; Parkin, S. S.; Felser, C.; Bernevig, B. A.; Regnault, N. All topological bands of all nonmagnetic stoichiometric materials. *Science* **2022**, *376*, eabg9094.
- [6] Zhang, P.; Chen, Y. Violation and revival of Kramers’ degeneracy in open quantum systems. *Phys. Rev. B* **2022**, *105*, L241106.
- [7] Ma, A.; Zhang, Y.; Christensen, T.; Po, H. C.; Jing, L.; Fu, L.; Soljacic, M. Topogivity: A machine-learned chemical rule for discovering topological materials. *Nano Letters* **2023**, *23*, 772–778.
- [8] Beltagy, I.; Lo, K.; Cohan, A. SciBERT: A Pretrained Language Model for Scientific Text. 2019; <https://arxiv.org/abs/1903.10676v3>, preprint.
- [9] Kresse, G.; Hafner, J. Ab initio molecular dynamics for liquid metals. *Phys. Rev. B* **1993**, *47*, 558–561.
- [10] Kresse, G.; Furthmüller, J. Efficiency of ab-initio total energy calculations for metals and semiconductors using a plane-wave basis set. *Computational Materials Science* **1996**, *6*, 15–50.
- [11] Kresse, G.; Joubert, D. From ultrasoft pseudopotentials to the projector augmented-wave method. *Phys. Rev. B* **1999**, *59*, 1758–1775.